PAUL SCHERRER INSTITUT

PSI Bericht Nr. 13-01
January, 2013
ISSN 1019-0643

Department Logistics
Division for Radiation Safety and Security

Aeroradiometric Measurements in the Framework of the Swiss Exercise ARM12

Gernot Butterweck, Benno Bucher, Ladislaus Rybach,
Georg Schwarz, Herbert Hödlmoser, Sabine Mayer,
Cristina Danzi and Gerald Scharding

PAUL SCHERRER INSTITUT

PSI Bericht Nr. 13-01
January, 2013
ISSN 1019-0643

Department Logistics
Division for Radiation Safety and Security

Aeroradiometric Measurements in the Framework of the Swiss Exercise ARM12

Gernot Butterweck[1], Benno Bucher[2], Ladislaus Rybach[3], Georg Schwarz[2], Herbert Hödlmoser[1], Sabine Mayer[1], Cristina Danzi[4], Gerald Scharding[4]

[1]Division for Radiation Safety and Security, Paul Scherrer Institute (PSI), 5232 Villigen PSI, Switzerland
[2]Swiss Federal Nuclear Safety Inspectorate (ENSI), Industriestrasse 19, 5200 Brugg, Switzerland
[3]Institut for Geophysics, Swiss Federal Institute of Technology Zürich (ETHZ), 8092 Zürich, Switzerland
[4]Swiss National Emergency Operations Center (NEOC), 8044 Zürich, Switzerland

Paul Scherrer Institut
5232 Villigen PSI
Switzerland
Tel. +41 56 310 21 11
Fax +41 56 310 21 99
www.psi.ch

ABSTRACT

The measurement flights of the exercise ARM12 were performed between June 25th and 29th. The exercise was organized by the National Emergency Operations Centre (NEOC) under coordination from the Expert Group for Aeroradiometrics (FAR). According to the alternating schedule of the annual ARM exercises, the environs of the nuclear power plants Leibstadt (KKL) and Beznau (KKB) were inspected together with the premises of the Paul Scherrer Institut (PSI) and the interim storage facility Zwischenlager Würenlingen AG (ZWILAG). As in previous years, the distinction between pressurised and boiling water reactor is clearly identified from the photon spectra. The intermediate storage facility ZWILAG could not be detected with airborne gamma-spectrometry. Due to the intersection of the flight line with air discharged from the stack of the accelerators located at the western part of the Paul Scherrer Institut (PSI) a clear signal is observed over PSI. The detected radionuclides are a controllled and permitted release from the stack of PSI West.

Measurement flights over Zurich city continued the series of baseline measurements over Swiss towns and cities. Both the results over Zurich and over the freight yard near Spreitenbach showed homogeneous results at background level.

The results of further measurements near Lac d'Emosson and Limmerensee reflect the alpine topography and local geological features.

A profile from Weinfelden to the Great St. Bernhard was measured to supplement the data base of Swiss aeroradiometric measurements. The results reflect changes in ground radiation and are characterised by the attenuation of photons from natural radionuclides in water bodies, glaciers and snow fields.

CONTENTS

TABLES

FIGURES

1 INTRODUCTION

Swiss airborne gamma spectrometry measurements started in 1986. Methodology and software for calibration, data acquisition and mapping were developed at the Institute of Geophysics of the Swiss Federal Institute of Technology Zurich (ETHZ). Between 1989 and 1993 the environs of Swiss nuclear installations were measured annually on behalf of the Swiss Federal Nuclear Safety Inspectorate (ENSI). This schedule was changed to biannual inspections in 1994, together with an organisational inclusion of the airborne gamma-spectrometric system into the Emergency Organisation Radioactivity (EOR) of the Federal Office for Civil Protection (FOCP). The deployment of the airborne gamma-spectrometric system is organized by the National Emergency Operations Centre (NEOC). NEOC is also responsible for the recruitment and instruction of the measurement team. Aerial operations are coordinated and performed by the Swiss Air Force. The gamma-spectrometric equipment is stationed at the military airfield of Dübendorf. The gamma-spectrometry system can be airborne within four hours. Responsibility for scientific support, development and maintenance of the aeroradiometric measurement equipment passed from ETHZ to the Radiation Metrology Section of the Paul Scherrer Institut (PSI) in 2003 in cooperation with ENSI. General scientific coordination and planning of the annual measuring flights is provided by the Expert Group for Aeroradiometrics (FAR). FAR was a working group of the Swiss Federal Commission for NBC-protection (ComNBC) and consists of experts from all Swiss institutions concerned with aeroradiometry. FAR was re-organized as an expert group of the NEOC in 2008. Additional information can be found at http://www.far.ensi.ch/.

1.1 Measuring System

The measuring system consists of four NaI-detectors with a total volume of 16.8 l. The spectrometer includes for each detector a 256-channel analyser with automatic gain control. The measurement control, data acquisition and storage are performed with an industrial grade personal computer. A second, identically configured PC is present in the electronics rack (Figure 1) as redundancy. Under normal operation conditions, this PC is used for real-time evaluation and mapping of the data. The positioning uses GPS (Global Positioning System) in the improved EGNOS (European Geostationary Navigation Overlay Service) mode. Together with spectrum and position, air pressure, air temperature and radar altitude are registered. The measuring system is mounted in an Aérospatiale AS 332 Super Puma helicopter of the Swiss Air Force (Figure 2). This helicopter has excellent navigation properties and allows emergency operation during bad weather conditions and nighttime. The detector is mounted in the cargo bay below the centre of the helicopter. The cargo bay is covered with a lightweight honeycomb plate to minimise photon absorption losses.

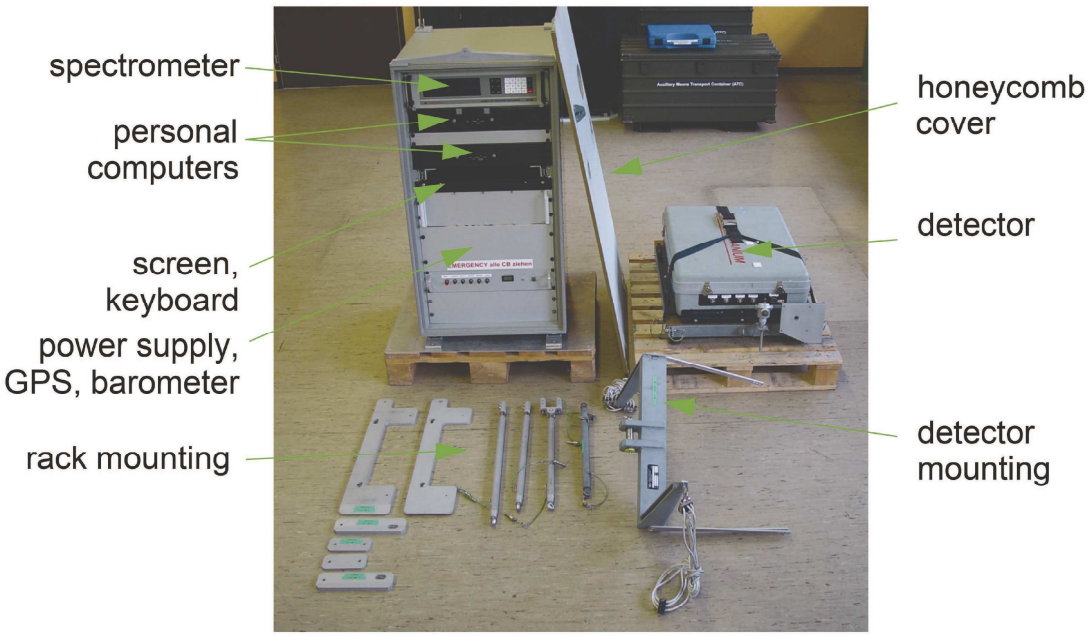

Figure 1: Measurement system of the Swiss team.

Figure 2: Super Puma Helicopter of the Swiss Air Force.

1.2 Measuring flights

The advantage of aeroradiometric measurements lies in the high velocity of measurements in a large area, even over rough terrain. Uniform radiological information of an area is obtained from a regular grid of measuring points. This grid is composed from parallel flight lines which are 100 m to 500 m apart, dependent on the scope of

the measurement. The flight altitude above ground is kept constant during the measuring flight. Typical values lie between 50 m and 100 m above ground. The spectra are recorded in regular time intervals of typical one second, yielding integration over 28 meters of the flight line at a velocity of 100 km/h.

1.3 Data evaluation

The data evaluation follows the methodology described in Schwarz (1991). Since the year 2000, software developed by the Research Group for Geothermics and Radiometry of the Institute of Geophysics of the Swiss Federal Institute of Technology Zurich (ETHZ) with on-line mapping options (Bucher, 2001) is used.

1.4 Data presentation

A first brief report (Kurzbericht) of the measurement results is compiled by the measurement team and published immediately after the end of the exercise on the homepage of NEOC. These reports are archived at http://www.far.ensi.ch.
Results of a further data evaluation are published in the form of a PSI-report. Starting with this report, a standardised and structured presentation is introduced. This targets an improvement in comparability between reports of different years and additional information concerning the quality of the data. For all measureing areas, a map of the total dose rate and the flight lines is presented together with a map of the Man-Made-Gross-Count (MMGC) ratio. As the MMGC-ratio is a very sensitive measure for the presence of artificial radionuclides, false positive values occur and have to be identified. In cases of high MMGC-ratio values, a map of the variation of the count rate in the MMGC high-energy window is depicted for rapid information on the quality of the MMGC-ratio. A map of the ^{232}Th activity concentration yields a second quality information as it can be expected that this quantity is constant over time.
If the MMGC-ratio indicates elevated values, maps of individual radionuclides are added based on the average photon spectrum over the affected area.

In the case of large changes of topography in the measured area, a map of the terrestrial dose rate consisting of the total dose rate reduced of the altitude dependent cosmic component is included. In the case of measuring flights with the main purpose of mapping natural radionuclide concentrations, a supplementary map of the ^{40}K activity concentration is presented.

As a last quality measure, an appendix with the basic parameters of the data evaluation is added to simplify a re-evaluation of the data in the future.

2 RESULTS OF THE MEASURING FLIGHTS DURING THE EXERCISE ARM12

The flights of the exercise ARM12 were performed with a Super Puma helicopter of the Swiss air force between June 25th and 29th. Personnel of the military unit Stab BR NAZ performed the measurements supported by experts from ENSI, PSI and NEOC. A short report with preliminary measurement results was placed on the NEOC website https://www.naz.ch/ on June 29th, 2012.

Flight parameters of ARM12 are listed in Table 1. Flight velocity of all measuring flights was around 30 m/s with a ground clearance of 90 m. The counting interval of the spectra was one second.

Table 1: Flight data of ARM12

Location	Flight number	Date	Effective measuring time [s]	Length of run [km]	Area [km^2]
KKB, KKL, PSI, Zwilag	2012006 2012018	25.6.2012 26.6.2012	9922	460	102
Zürich	2012011 2012012 2012019 2012020	26.6.2012 26.6.2012 27.6.2012 27.6.2012	14743	639	81
Lac d'Emosson Finhaut La Crêta	2012022 2012023 2012024	28.6.2012	2493	89	13
Spreitenbach	2012026	28.6.2012	915	42	7
Limmerensee	2012027	28.6.2012	2293	56	9
Profile Weinfelden – Great St. Bernhard	2012021	28.6.2012	6464	267	-

2.1 Recurrent measurement area around KKL, KKB, PSI and ZWILAG

According to a biannual rotation of routine measurements, the environs of the nuclear power plants Leibstadt (KKL) and Beznau (KKB), together with the premises of the Paul Scherrer Institut (PSI) and the interim storage facility Zwischenlager Würenlingen AG (ZWILAG) were inspected in 2012.

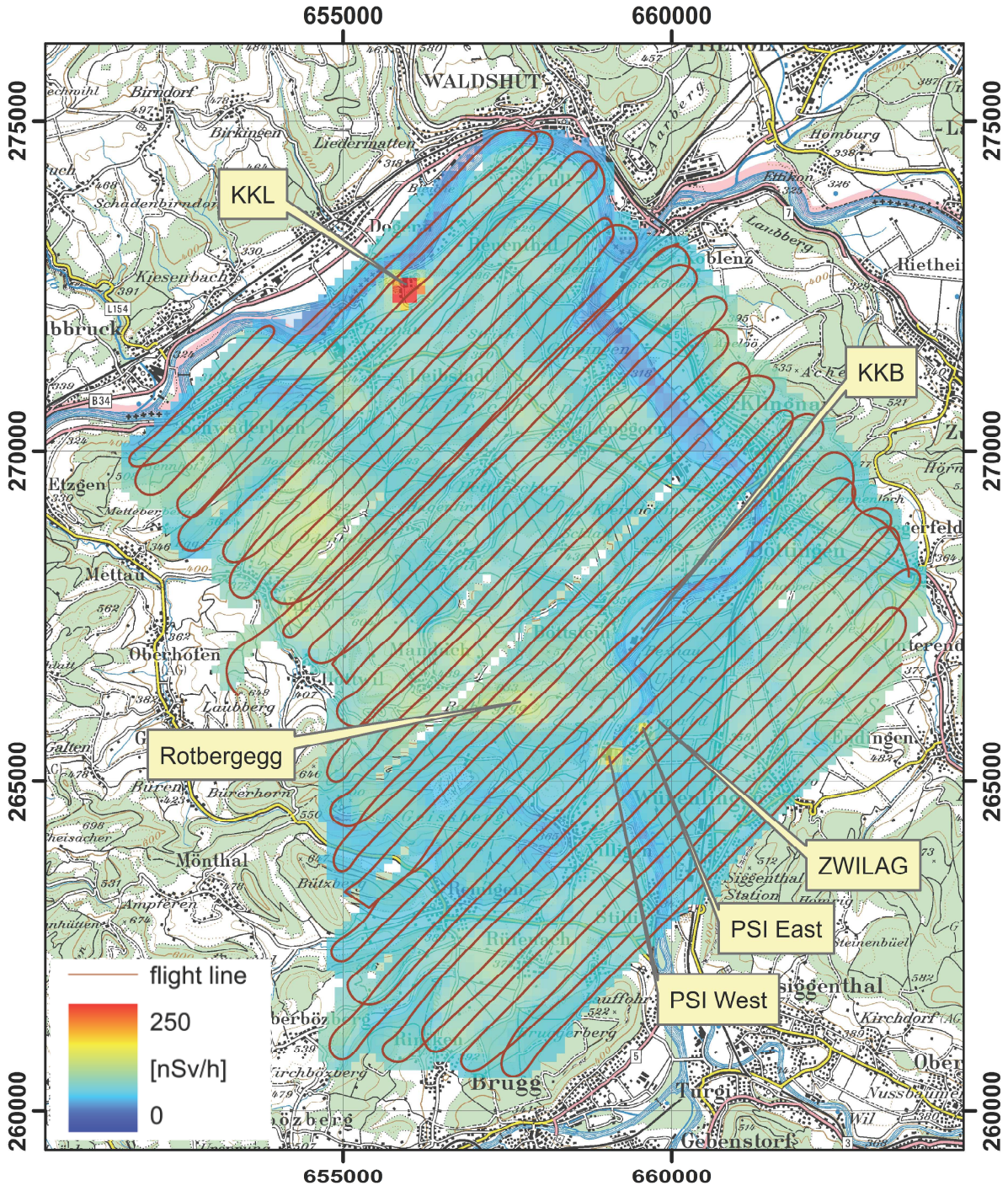

Figure 3: Dose rate in the vicinity of KKL, KKB, PSI and ZWILAG. PK100 © 2012 swisstopo (JD100042)

The map of the dose rate shows elevated values over KKL, PSI and the Rotbergegg, whereas KKB and ZWILAG are unobstrusive (Figure 3).

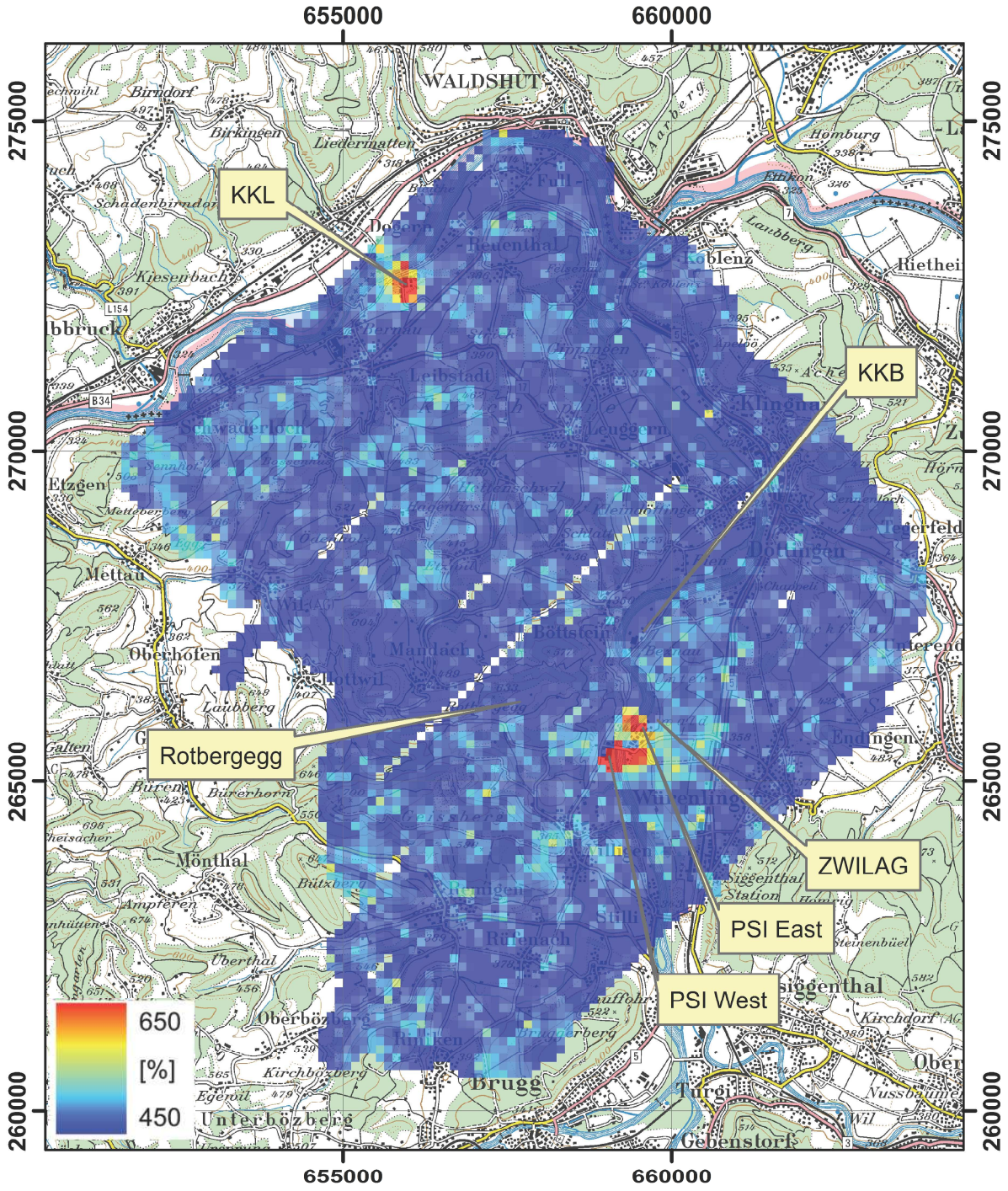

Figure 4: MMGC ratio in the vicinity of KKL, KKB, PSI and ZWILAG. PK100 © 2012 swisstopo (JD100042)

The map of the MMGC ratio (Figure 4) depicts elevated values over KKL and both parts of PSI. The spot with elevated dose rate values at Rotbergegg does not show in the map of the MMGC ratio, indicating that the dose rate increase was caused by naturally occuring radioactive material (NORM).

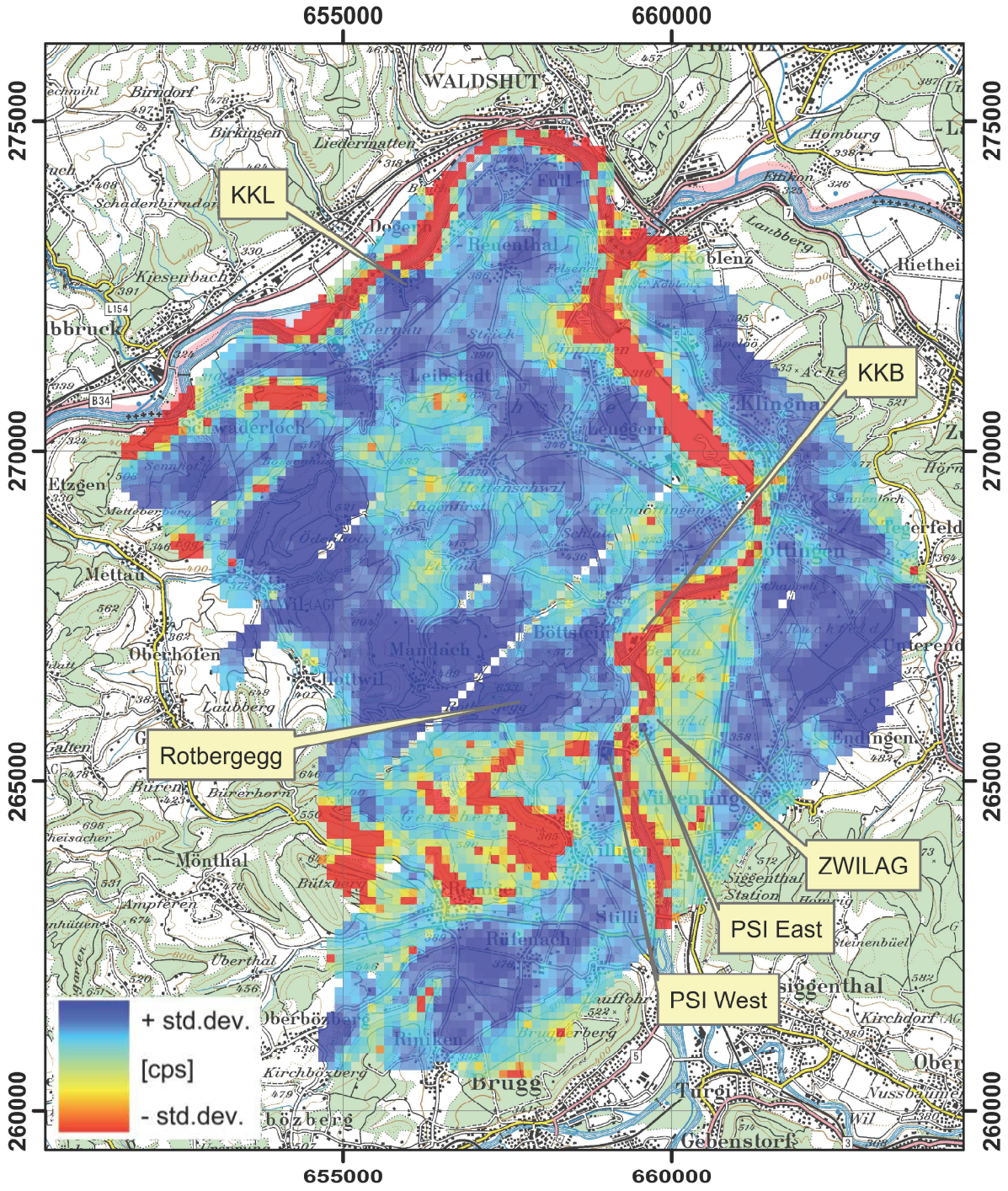

Figure 5: Variation of the count rate in the MMGC high energy window in the vicinity of KKL, KKB, PSI and ZWILAG.
PK100 © 2012 swisstopo (JD100042)

The map of the variation of the count rate in the MMGC high energy window (Figure 5) denotes unsual low values in red. These areas are prone to false positive indications of the MMGC ratio (Figure 4). As the elevated values of the MMGC ratio at KKL and both sites of PSI do not coincide with unusual low values of the MMGC high energy count rate, they have to be analysed in more detail.

The elevated dose rate over the premises of KKL is caused by high energy photon radiation of the activation product ^{16}N. These photons lose energy due to Compton scattering in the air between power plant and helicopter, causing an increased count rate in the whole energy range compared to a background spectrum (Figure 6). Photon radiation with energies above 1022 keV is able to generate electron-positron pairs. As a positron is the anti-particle of an electron, both annihilate under emission of two photons with energy of 511 keV. This annihilation peak can also be observed in the spectrum.

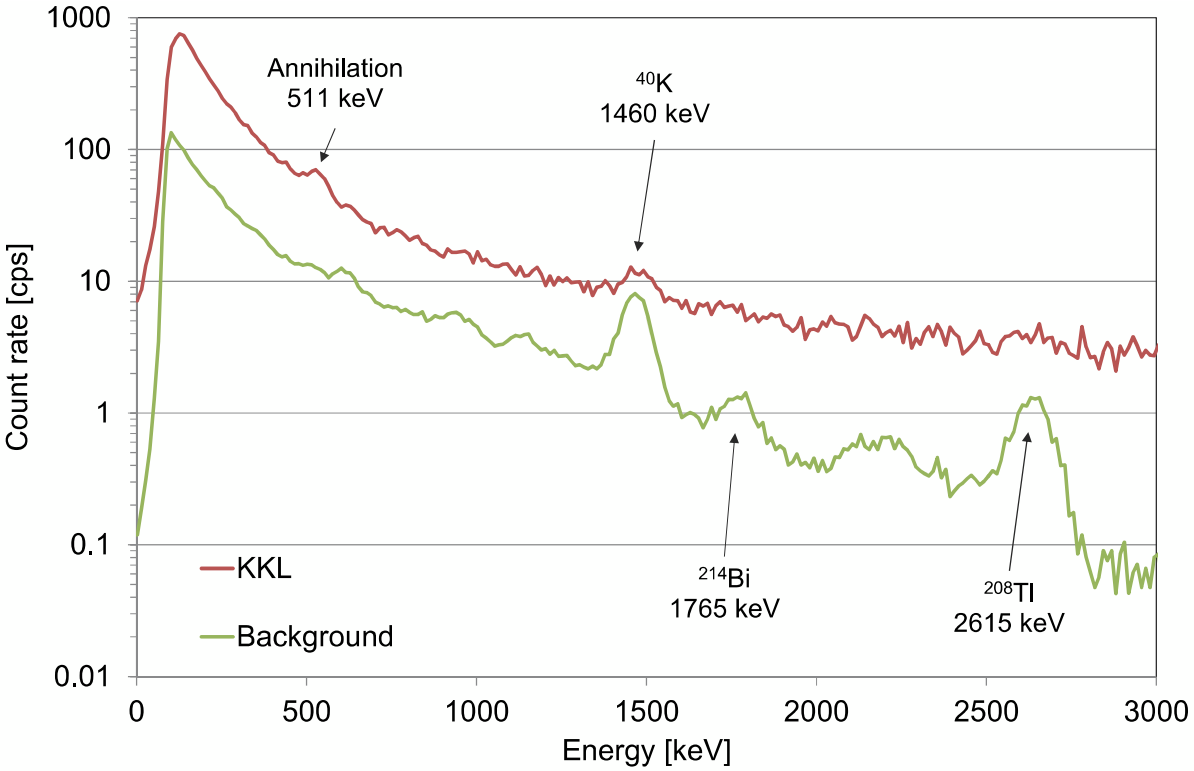

Figure 6: Comparison of the photon spectrum over the KKL premises to a background spectrum.

The elevated dose rate over the facilities of PSI is mainly due to radioactive gases produced in the accelerators of the PSI West site. These gases are a controlled and permitted release from the stack of PSI West. The released gas mixture contains the positron emitting Isotopes ^{15}O (67%), ^{11}C (16%), ^{13}N (16%) and ^{18}F (1%) and the beta emitter ^{41}Ar. Apart from photon emissions of natural radionuclides, the annihilation radiation at 511 keV is clearly detectable in the spectra measured above both parts of PSI (Figure 7). The 1294 keV photon peak of ^{41}Ar is visible over the PSI West area, whereas over the PSI East area ^{60}Co from the Federal Intermediate Storage Facility (Bundeszwischenlager BZL) is indicated.

The spectrum over the area with elevated dose rate at the Rotbergegg shows clearly photon emissions of radionuclides of the thorium decay series (Figure 8). Thus this location can be identified in the map of the ^{232}Th activity concentration (Figure 9).

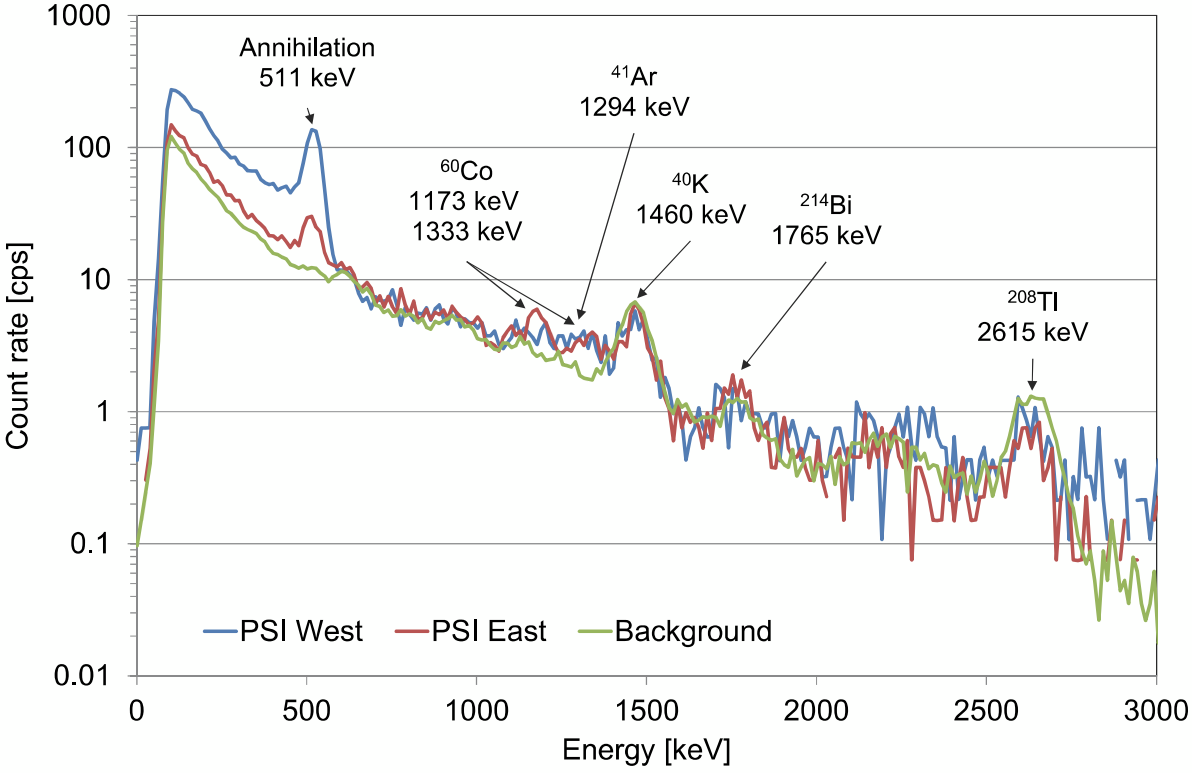

Figure 7: Comparison of the photon spectrum over the PSI premises to a background spectrum.

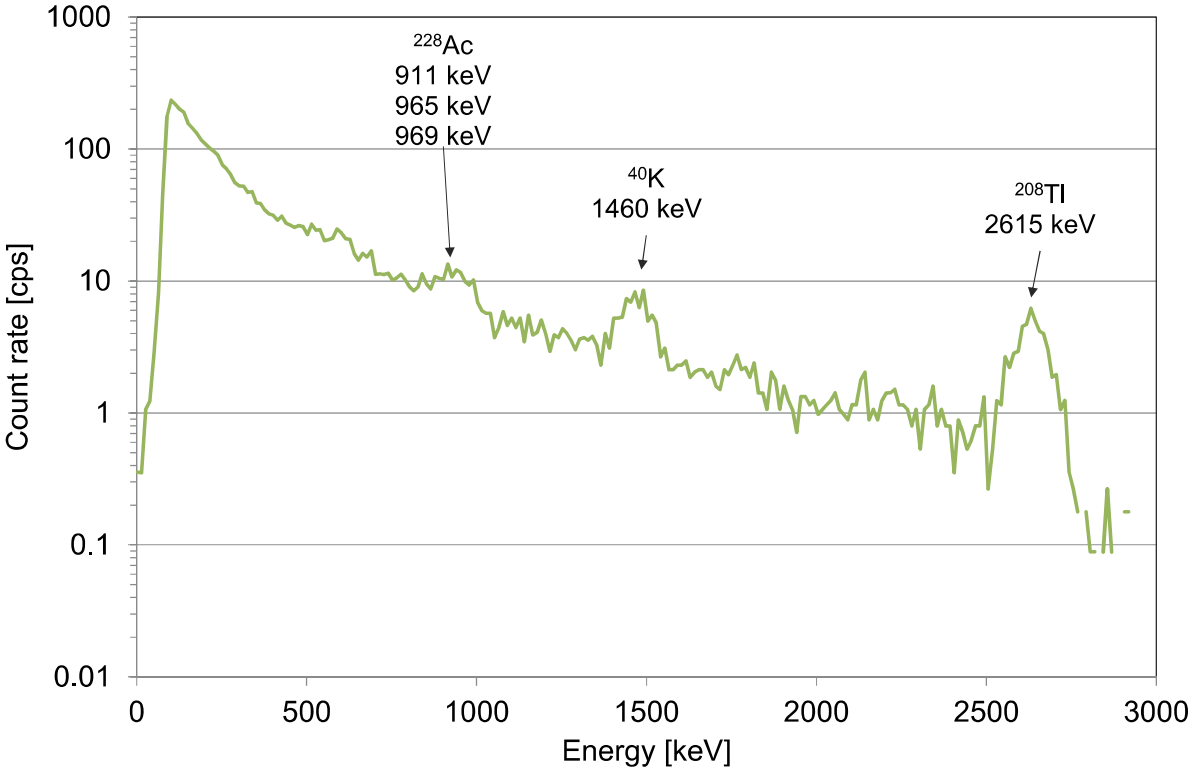

Figure 8: Photon spectrum over Rotbergegg.

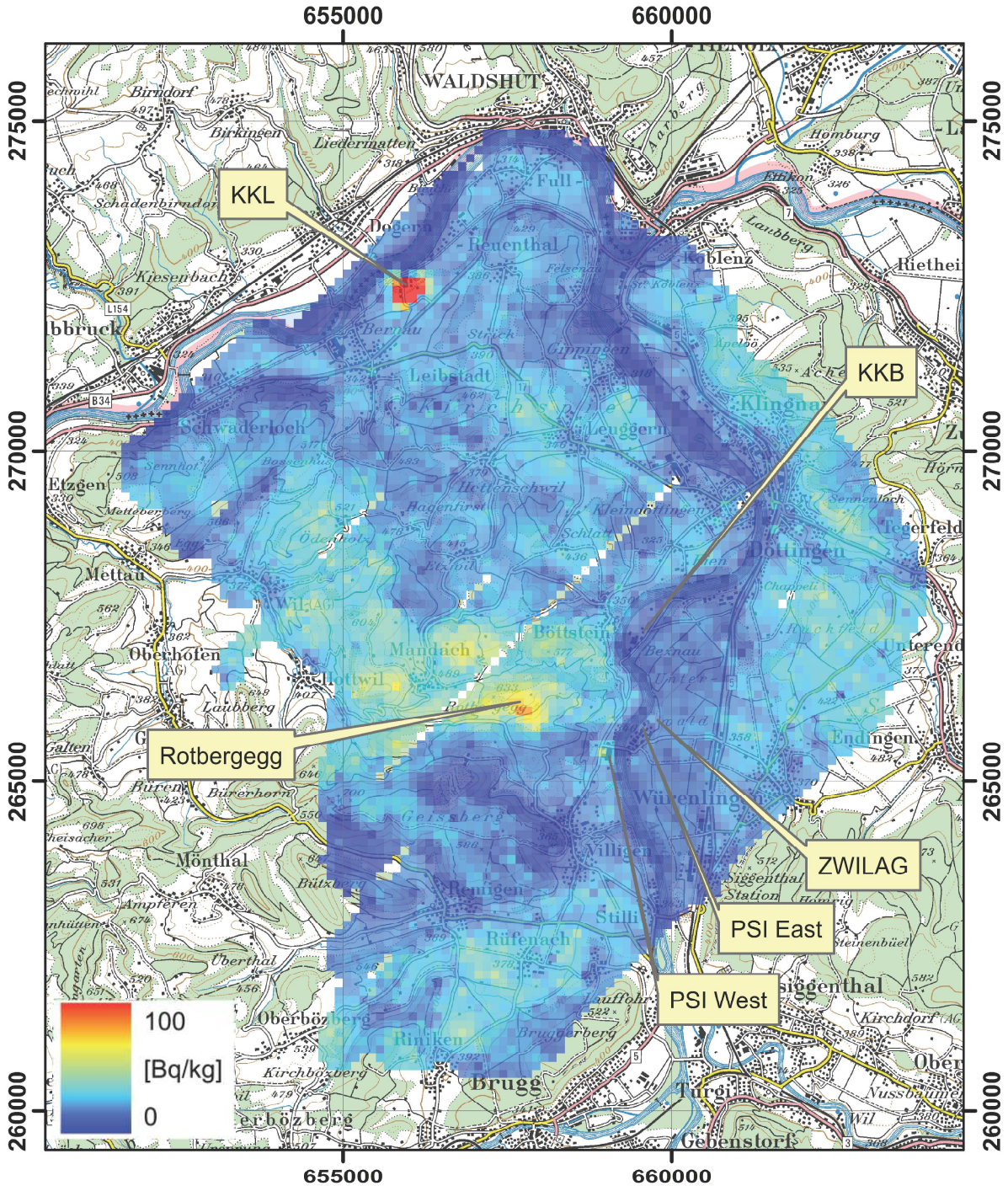

Figure 9: ^{232}Th activity concentration in the vicinity of KKL, KKB, PSI and ZWILAG. PK100 © 2012 swisstopo (JD100042)

The map of the ^{232}Th activity concentration (Figure 9) shows elevated values over the premises of KKL due to a misinterpretation of scattered photon radiation of ^{16}N. The elevated ^{232}Th concentrations at Rotbergegg have been observed already in previous years. The anomaly was confirmed by ground measurements with in-situ gamma-spectrometry.

2.2 Zurich

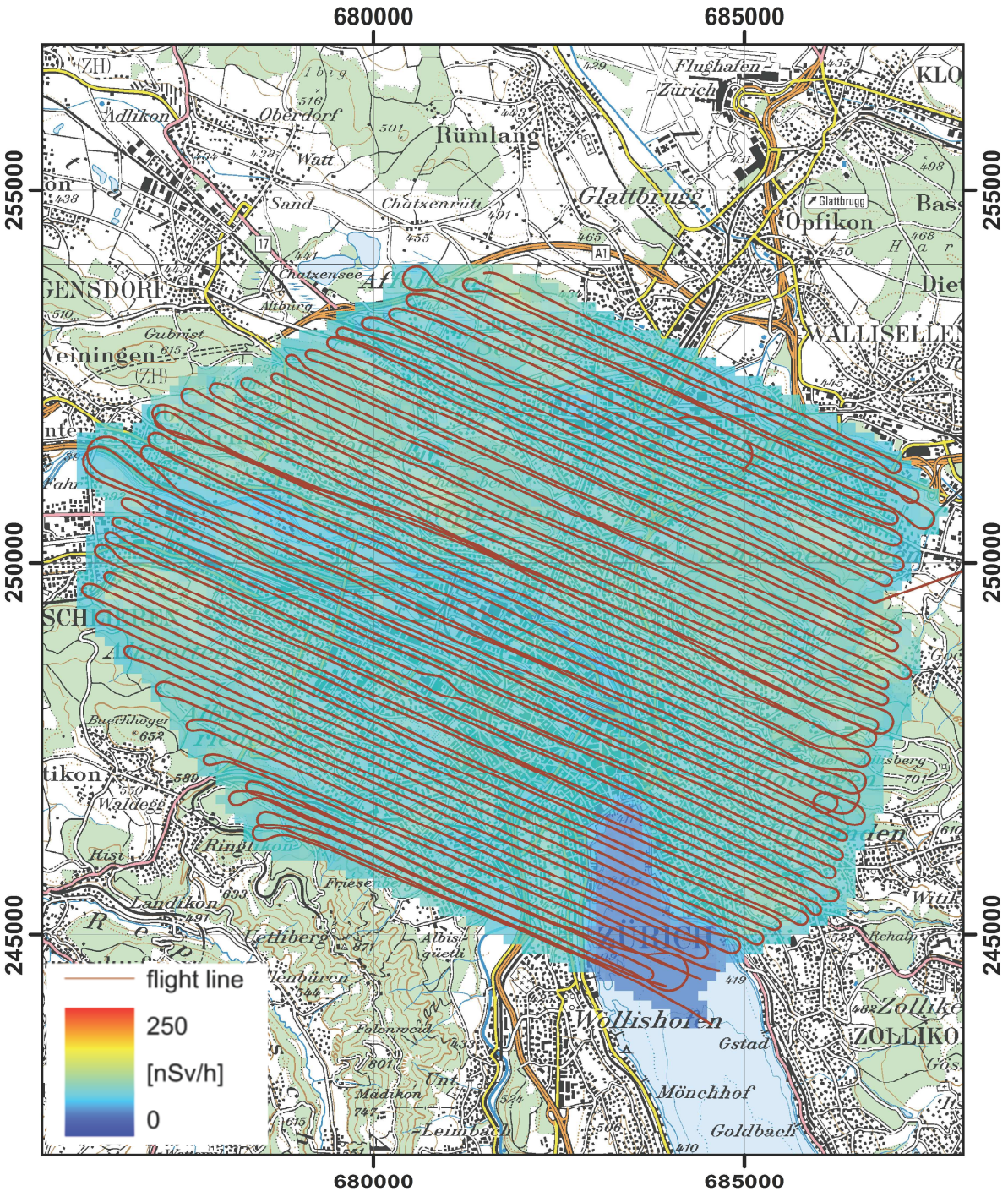

Figure 10: Dose rate over Zurich city. PK100 © 2012 swisstopo (JD100042)

With the exception of low dose rate values over Lake Zurich due to the absorption of terrestric photon radiation in the water layer, the map of the total dose rate (Figure 10) yields a uniform picture at typical environmental dose rate levels. Due to a temporary malfunction of the GPS receiver, some flight lines deviate from the scheduled path.

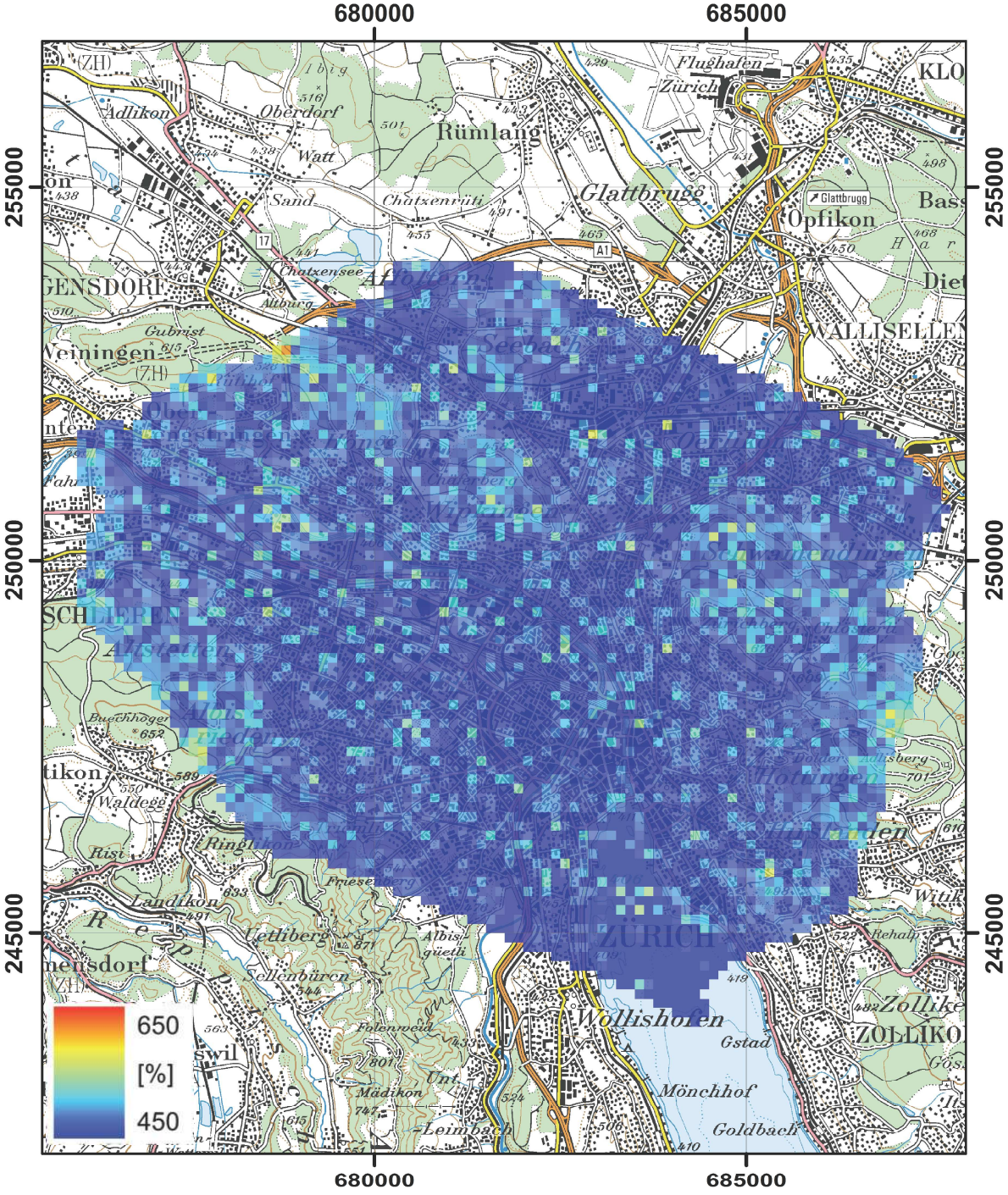

Figure 11: MMGC ratio over Zurich city. PK100 © 2012 swisstopo (JD100042)

Analog to the map of the total dose rate (Figure 10), the map of the MMGC ratio (Figure 11) does not present any unexpected features.

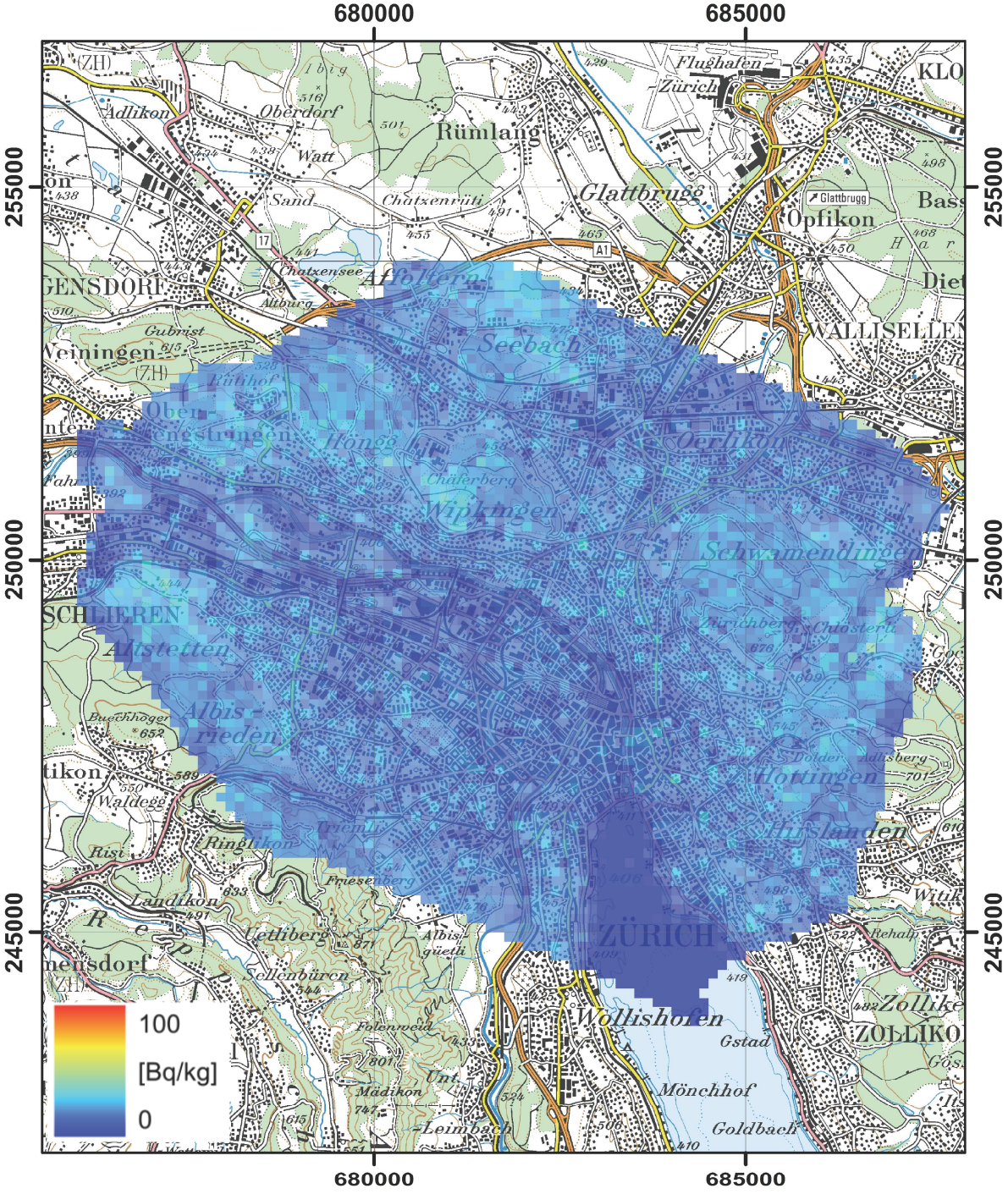

Figure 12: ^{232}Th activity concentration over Zurich city.
PK100 © 2012 swisstopo (JD100042)

With the exception of low values over Lake Zurich due to the absorption of the photon radiation originating from the ^{232}Th decay series in the water layer, the map of the ^{232}Th activity concentration (Figure 12) yields a uniform picture at typical environmental dose rate levels.

2.3 Lac d'Emosson, Finhaut and La Crêta

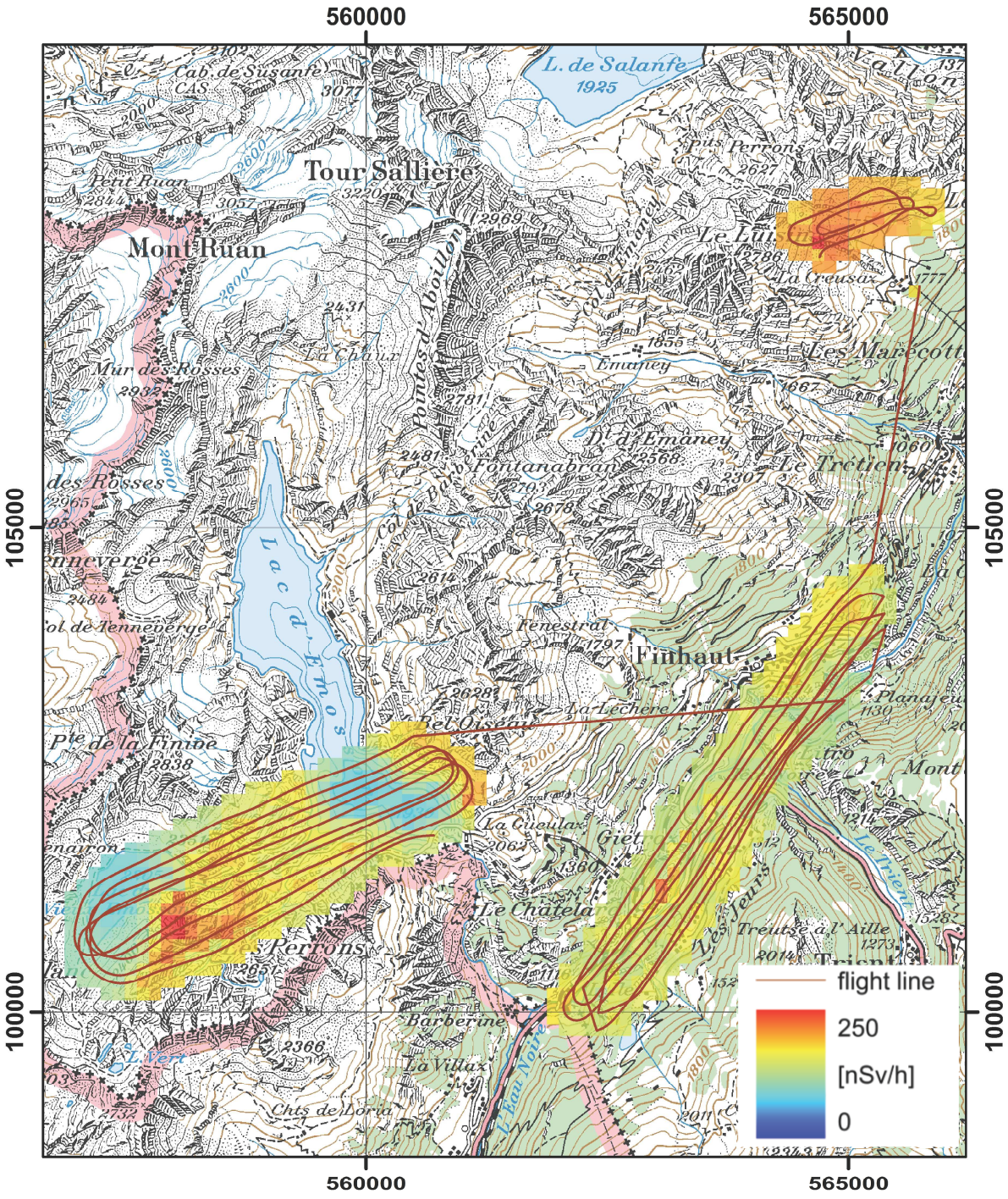

Figure 13: Dose rate in the vicinity of Lac d'Emosson.
PK100 © 2012 swisstopo (JD100042)

The map of the total dose rate (Figure 13) shows several distinct features due to topographical effects in this alpine region, local water bodies and geological features.

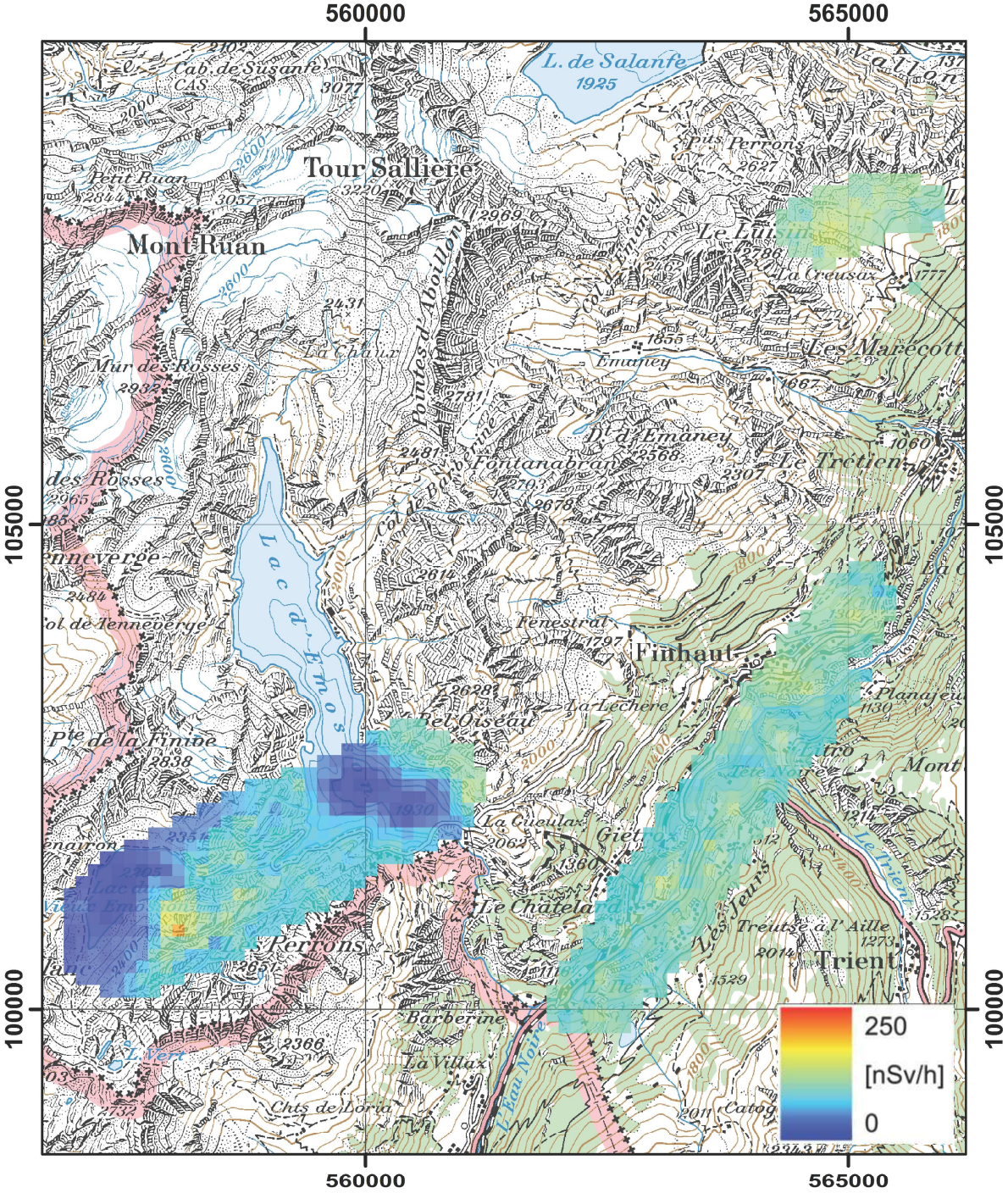

Figure 14: Terrestrial component of the dose rate in the vicinity of Lac d'Emosson. PK100 © 2012 swisstopo (JD100042)

The subtraction of the cosmic component of the total dose rate, rendering the terrestrial component of the total dose rate (Figure 14), reveals that most features observed in the map of the total dose rate (Figure 13) are due to the alpine nature of the measurement area.

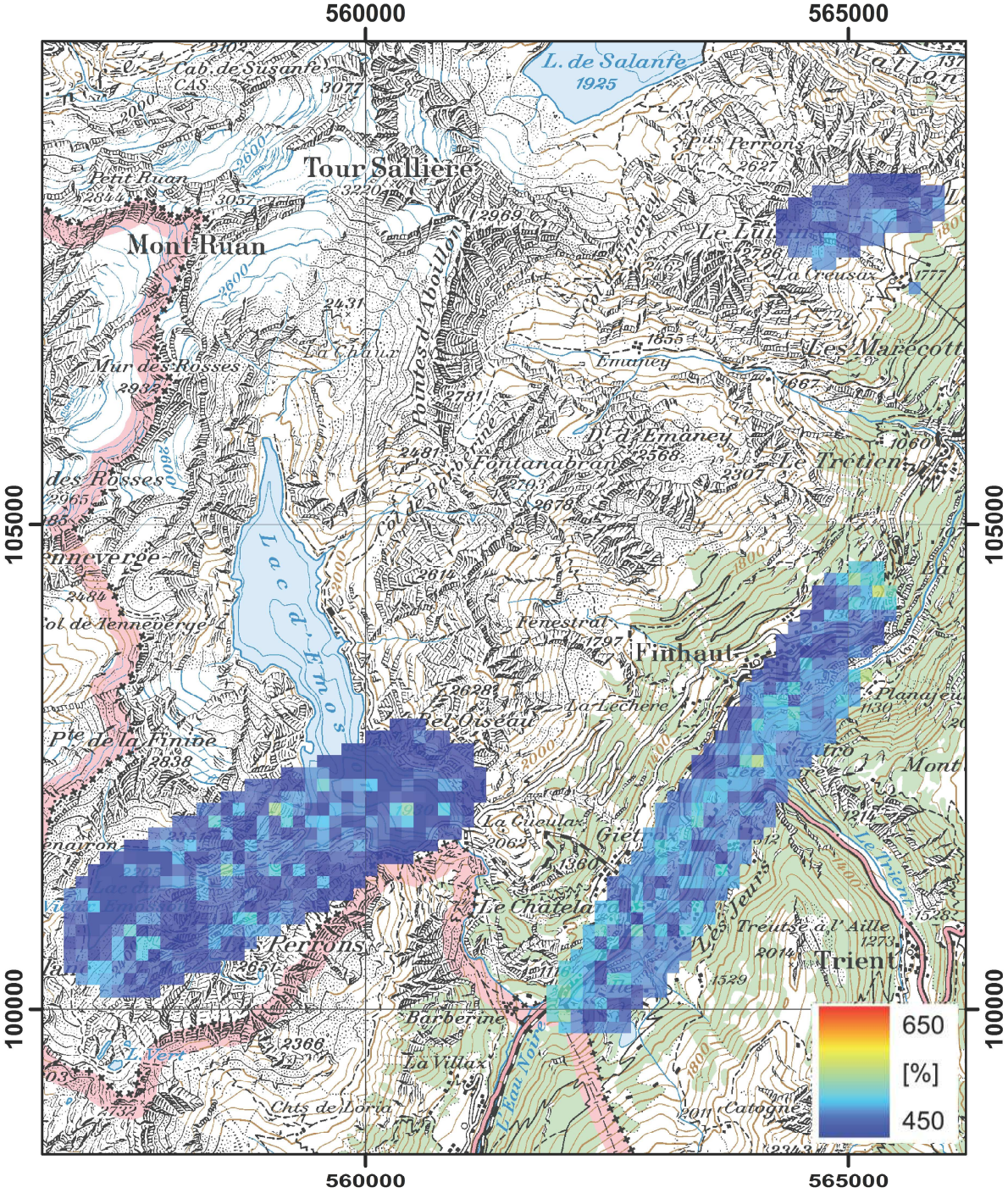

Figure 15: MMGC-Ratio in the vicinity of Lac d'Emosson.
PK100 © 2012 swisstopo (JD100042)

The map of the MMGC-ratio (Figure 15) without significantly elevated values at the locations of higher terrestrial dose rate (Figure 14) leads to the conclusion that the increased dose rate is caused by natural radionuclides.

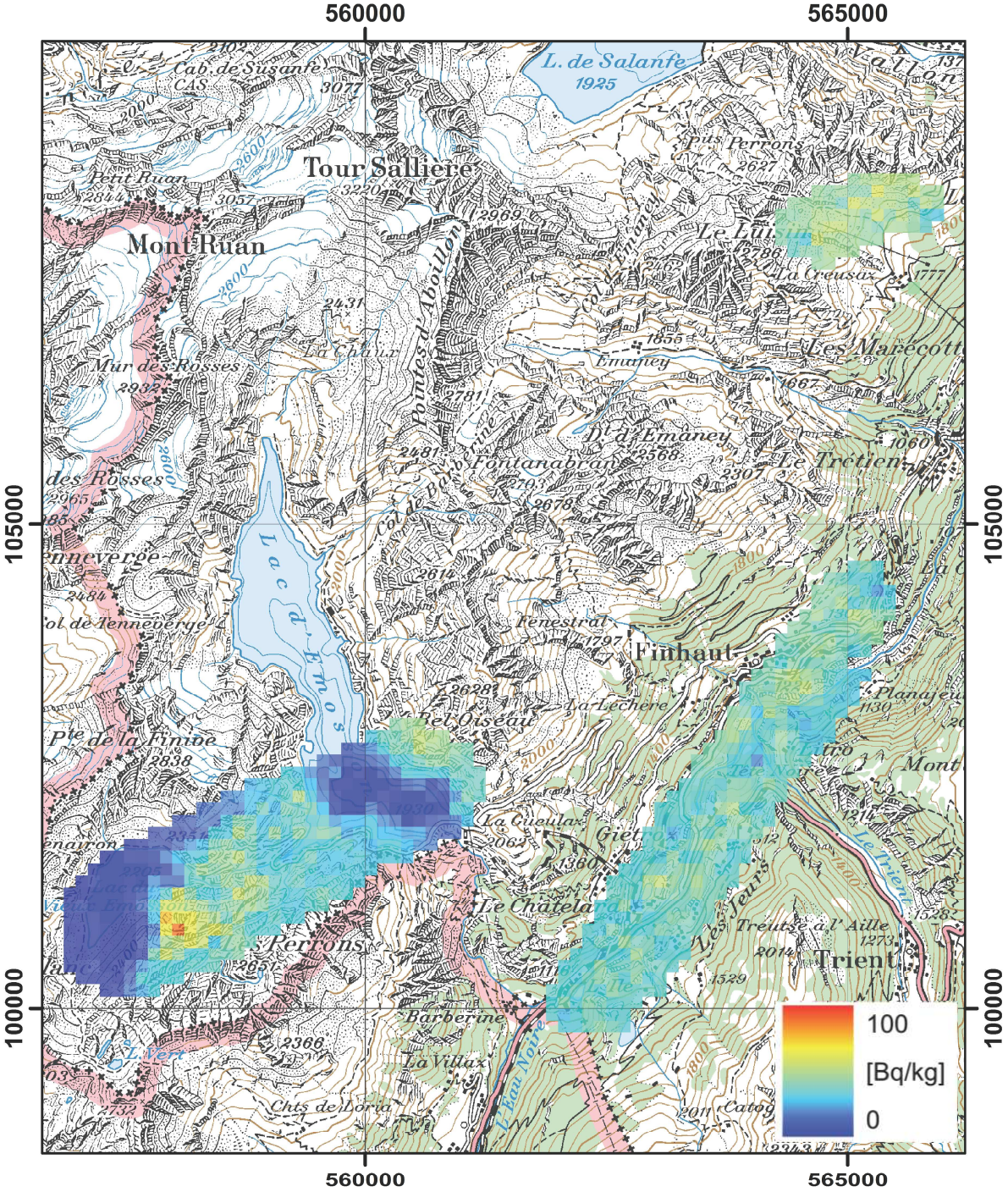

Figure 16: ^{232}Th activity concentration in the vicinity of Lac d'Emosson. PK100 © 2012 swisstopo (JD100042)

The map of the ^{232}Th activity concentration (Figure 16) shows a pattern similar to the map of the terrestrial dose rate (Figure 14).

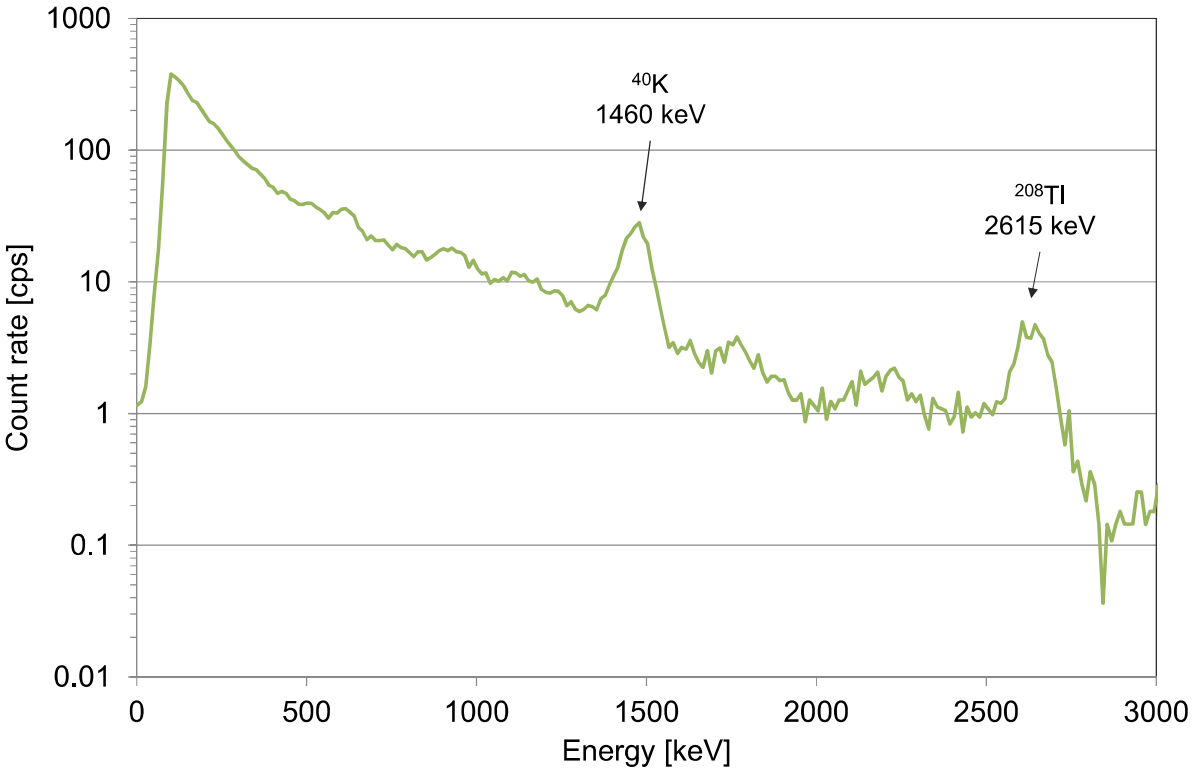

Figure 17: Photon spectrum over the area with elevated ^{232}Th activity concentrations at coordinate 558070, 100810.

The photon spectrum over the spot with elevated ^{232}Th activity concentration (Figure 17) located at Swiss National Coordinates (558070, 100810) confirms that the increase of the dose rate is caused by the natural radionuclides ^{40}K and the decay series of ^{232}Th.

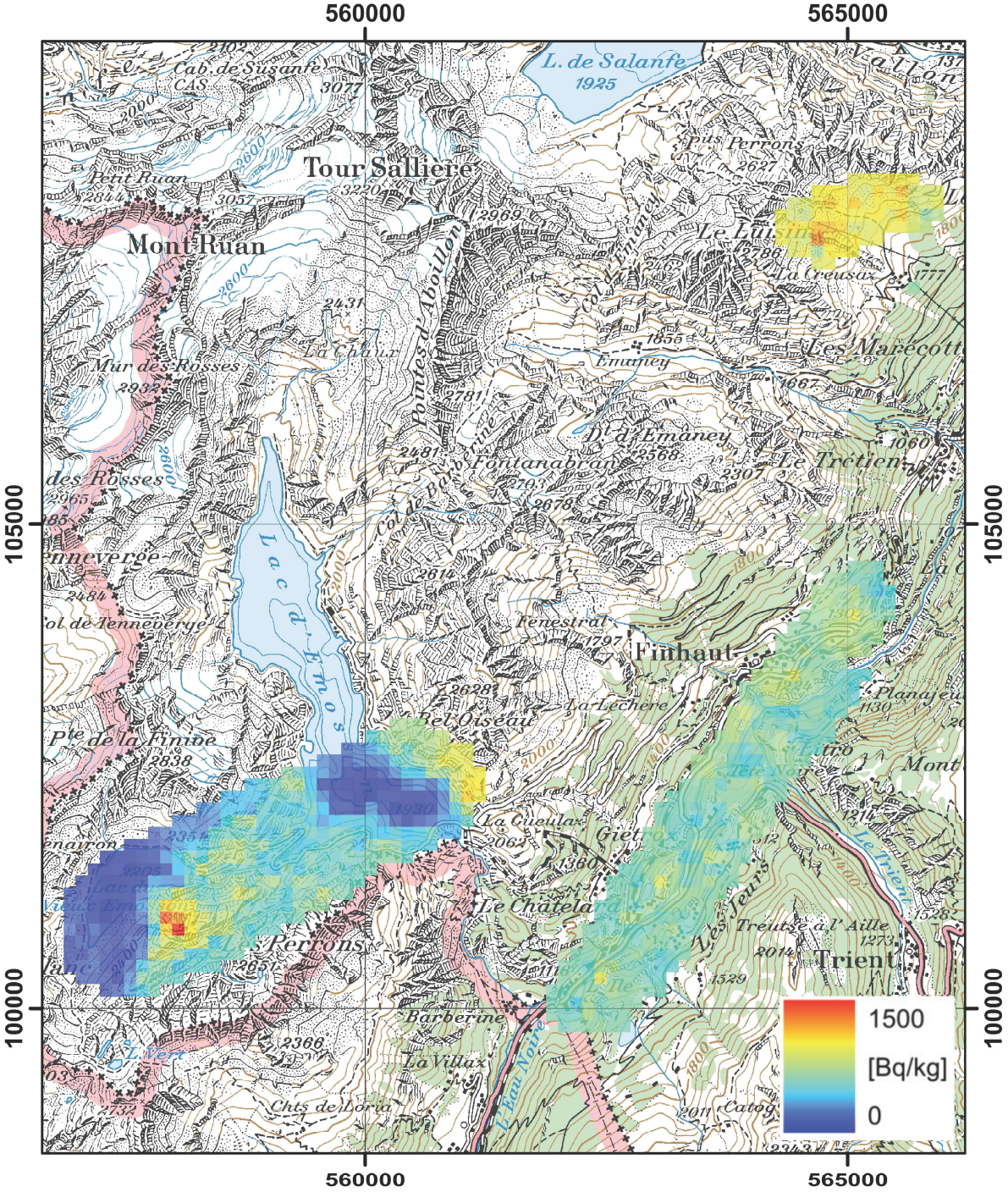

Figure 18: ^{40}K activity concentration in the vicinity of Lac d'Emosson. PK100 © 2012 swisstopo (JD100042)

As expected from the photon spectrum (Figure 17), the spot at coordinate (558070, 100810) shows also elevated activity concentrations of ^{40}K (Figure 18).

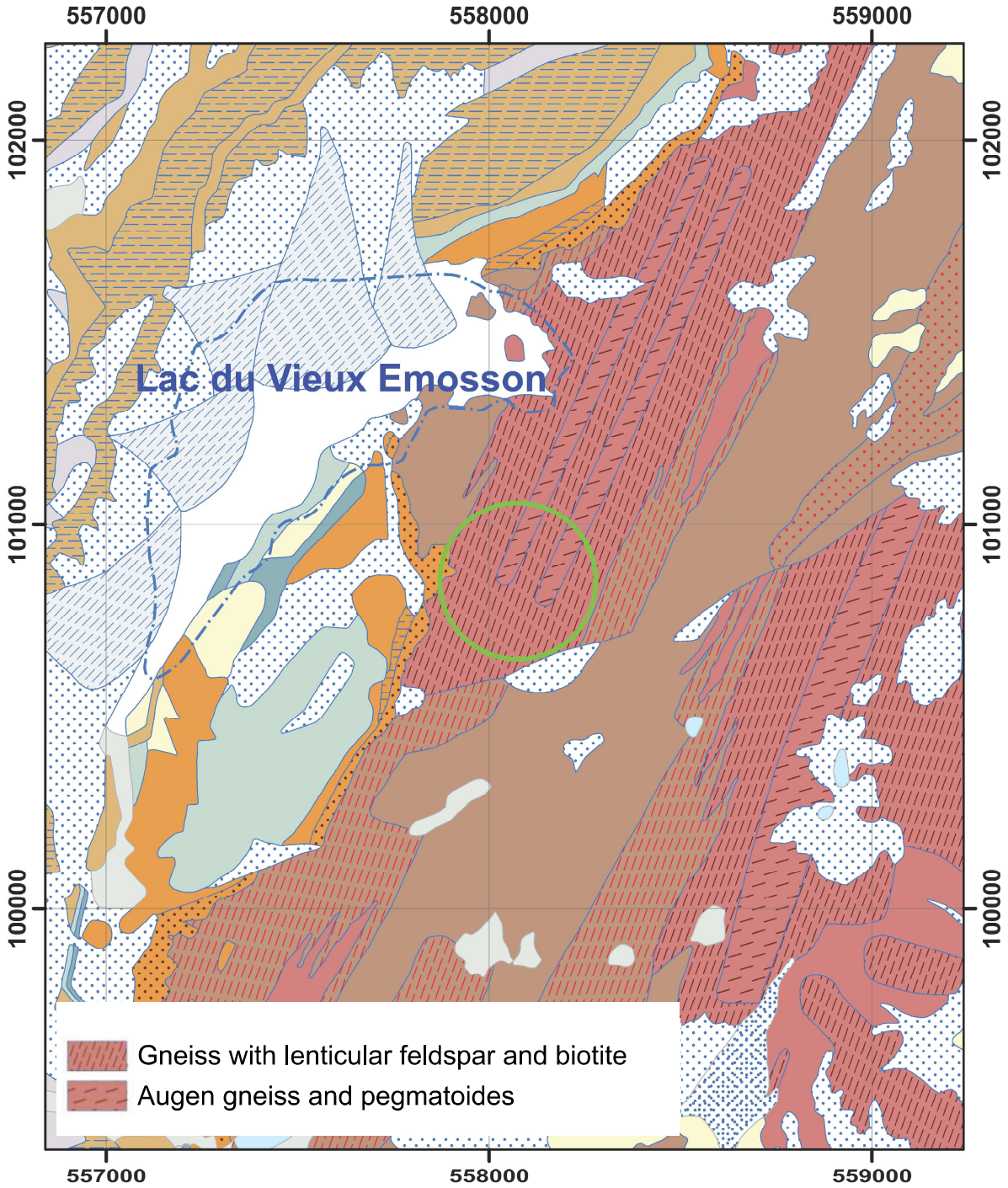

Figure 19: Geological map of the area near Lac du Vieux Emosson. The area with high ^{232}Th and ^{40}K activity concentration is denoted with a green circle. GeoCover © 2012 swisstopo (JD100042)

The region with elevated ^{232}Th and ^{40}K activity concentrations corresponds with the southern end of an intrusion zone of different gneisses (Figure 19). Labhart and Rybach (1974) reported enrichment of radionuclides in the border zones of intrusions. Unfortunately, a second similar structure at coordinate (558654, 99770) was not included in the measurement area.

2.4 Spreitenbach

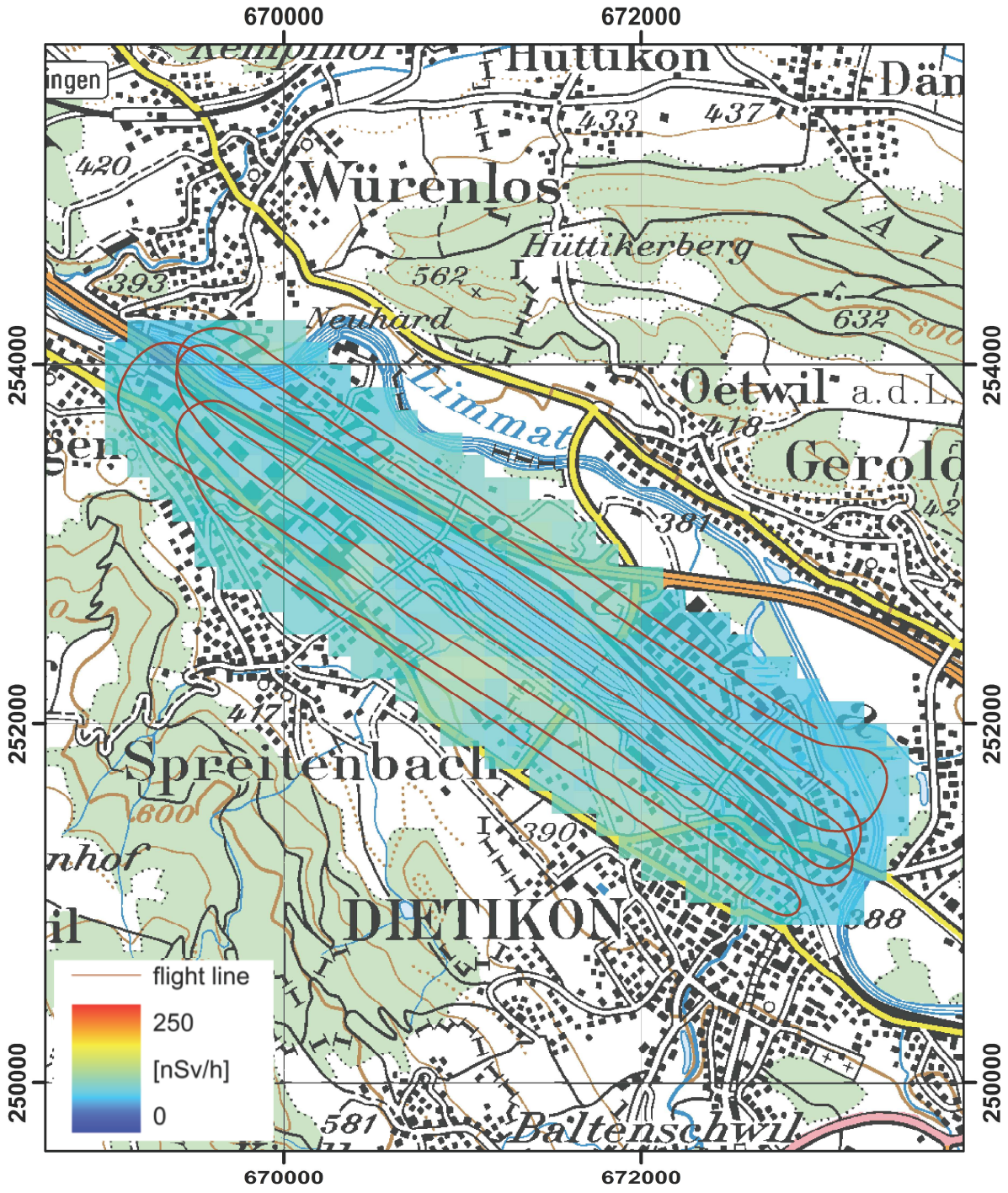

Figure 20: Dose rate near Spreitenbach.
PK100 © 2012 swisstopo (JD100042)

The total dose rate measured at the freight yard at Spreitenbach displays normal values over the complete area (Figure 20).

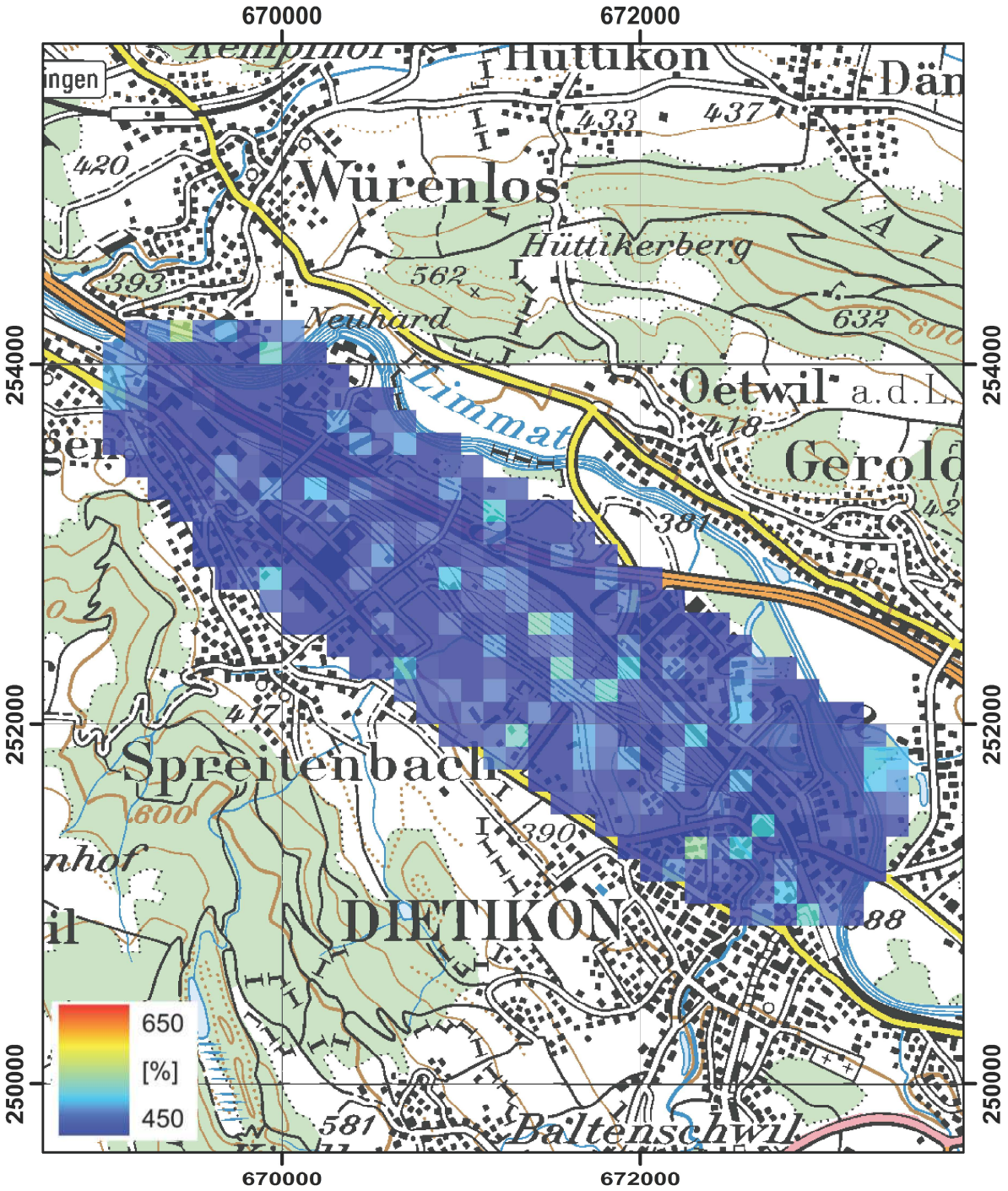

Figure 21: MMGC-ratio near Spreitenbach.
PK100 © 2012 swisstopo (JD100042)

The MMGC ratio measured at the freight yard at Spreitenbach yields no indication of the presence of artificial radionuclides (Figure 21).

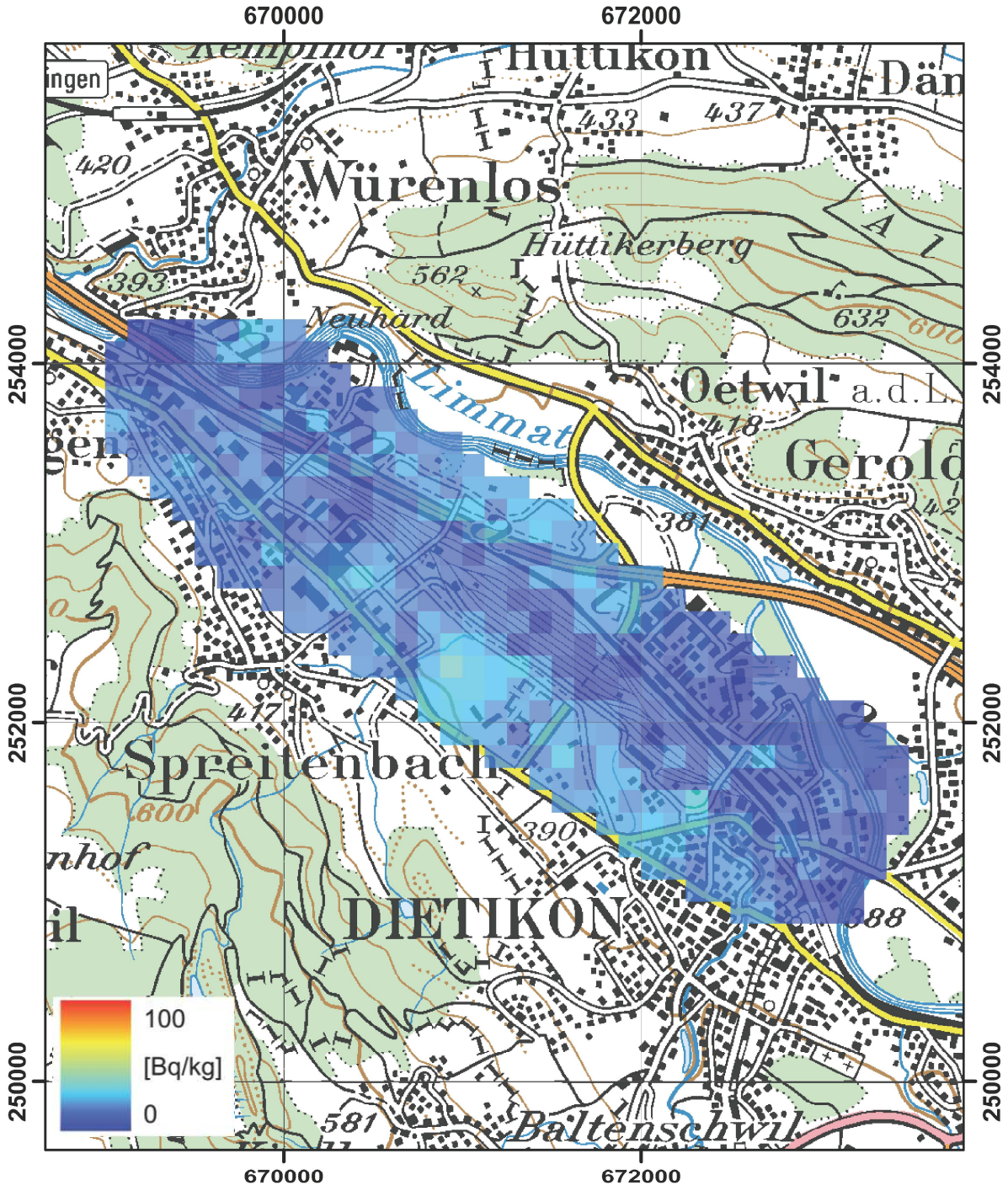

Figure 22: ^{232}Th activity concentration near Spreitenbach.
PK100 © 2012 swisstopo (JD100042)

The ^{232}Th activity concentration at the freight yard at Spreitenbach is low throughout the complete measurement area (Figure 22).

2.5 Limmerensee

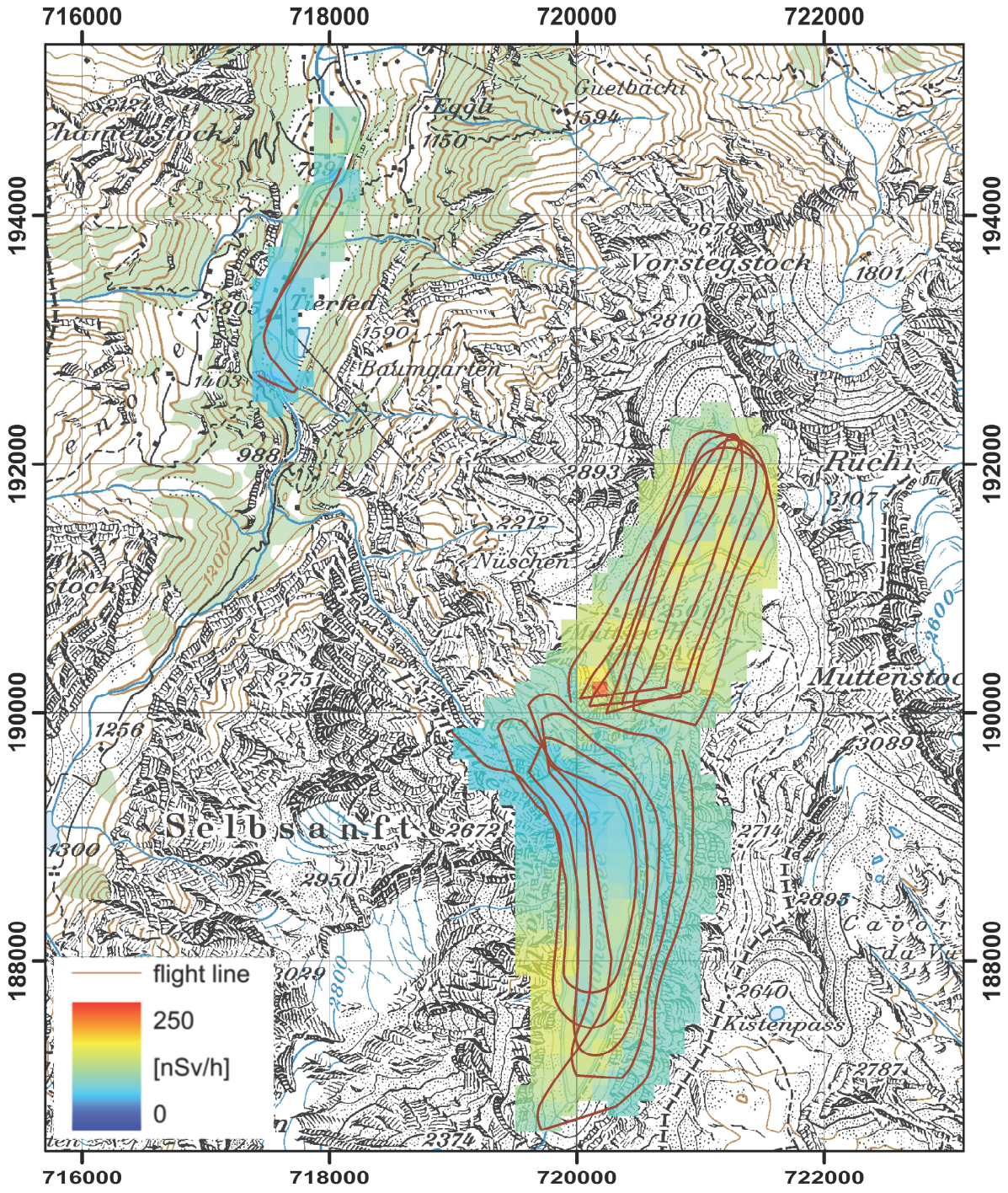

Figure 23: Dose rate in the vicinity of Limmerensee.
PK100 © 2012 swisstopo (JD100042)

The alpine location of the Limmerensee influences the map of the total dose rate (Figure 23).

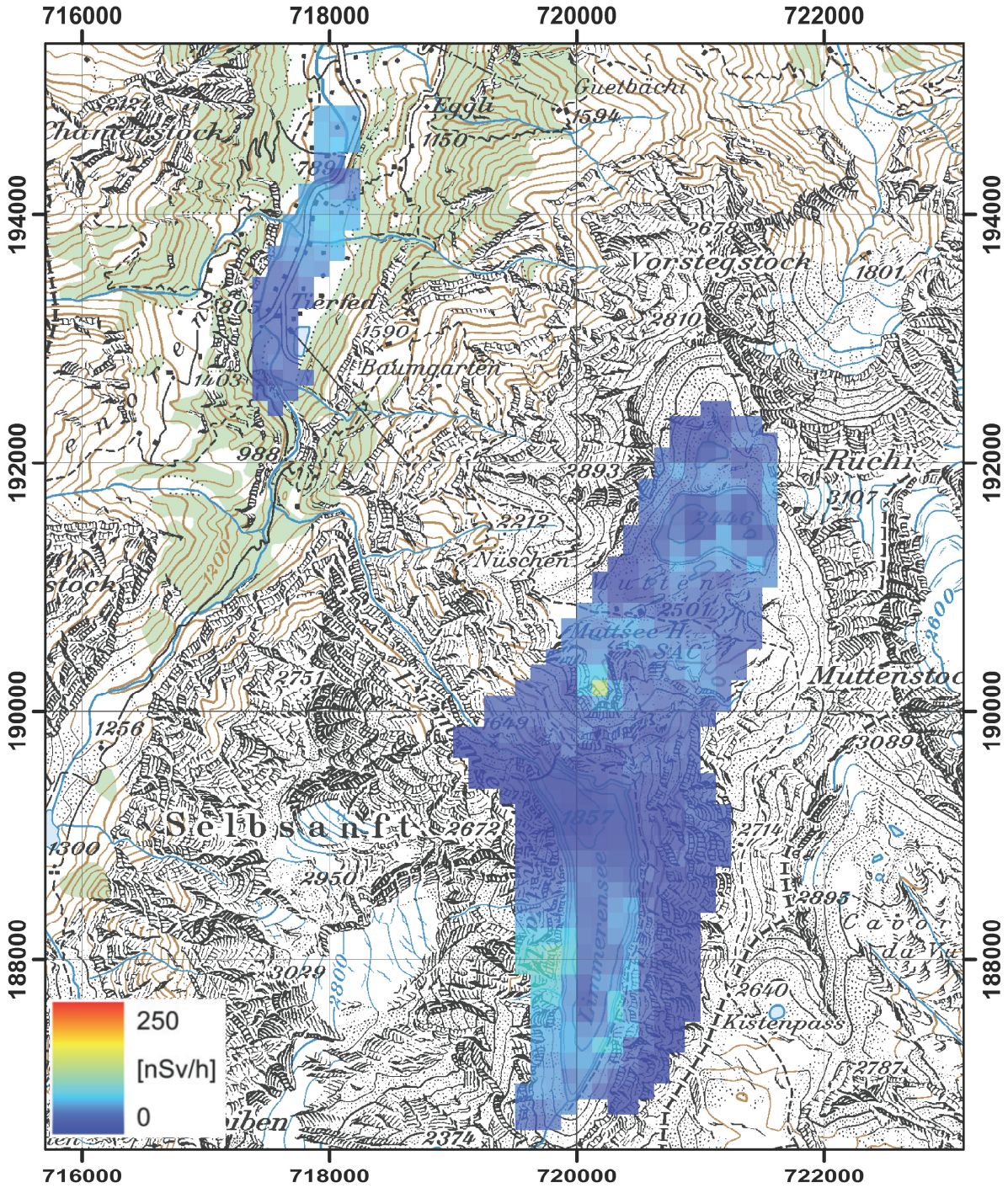

Figure 24: Terrestrial component of the dose rate in the vicinity of Limmerensee. PK100 © 2012 swisstopo (JD100042)

The terrestrial component of the dose rate (Figure 24) is uninfluenced from the height dependent cosmic dose rate and gives thus a better indication of radionuclide content of the rock formations.

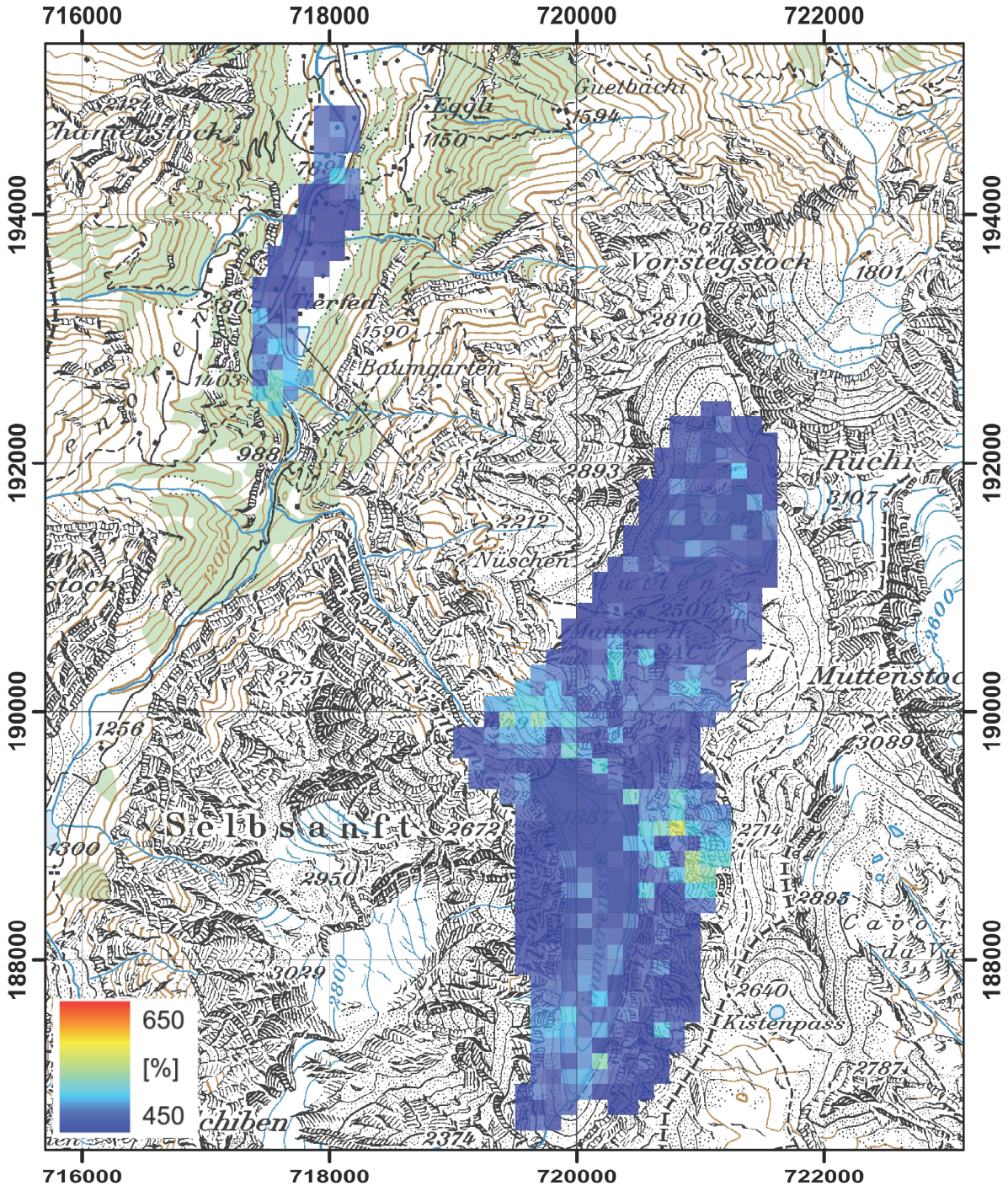

Figure 25: MMGC-ratio in the vicinity of Limmerensee.
PK100 © 2012 swisstopo (JD100042)

Elevated values in the MMGC-ratio (Figure 25) do not correspond to elevated values of the terrestrial component of the dose rate (Figure 24), suggesting an artifact of this very sensitive quantity.

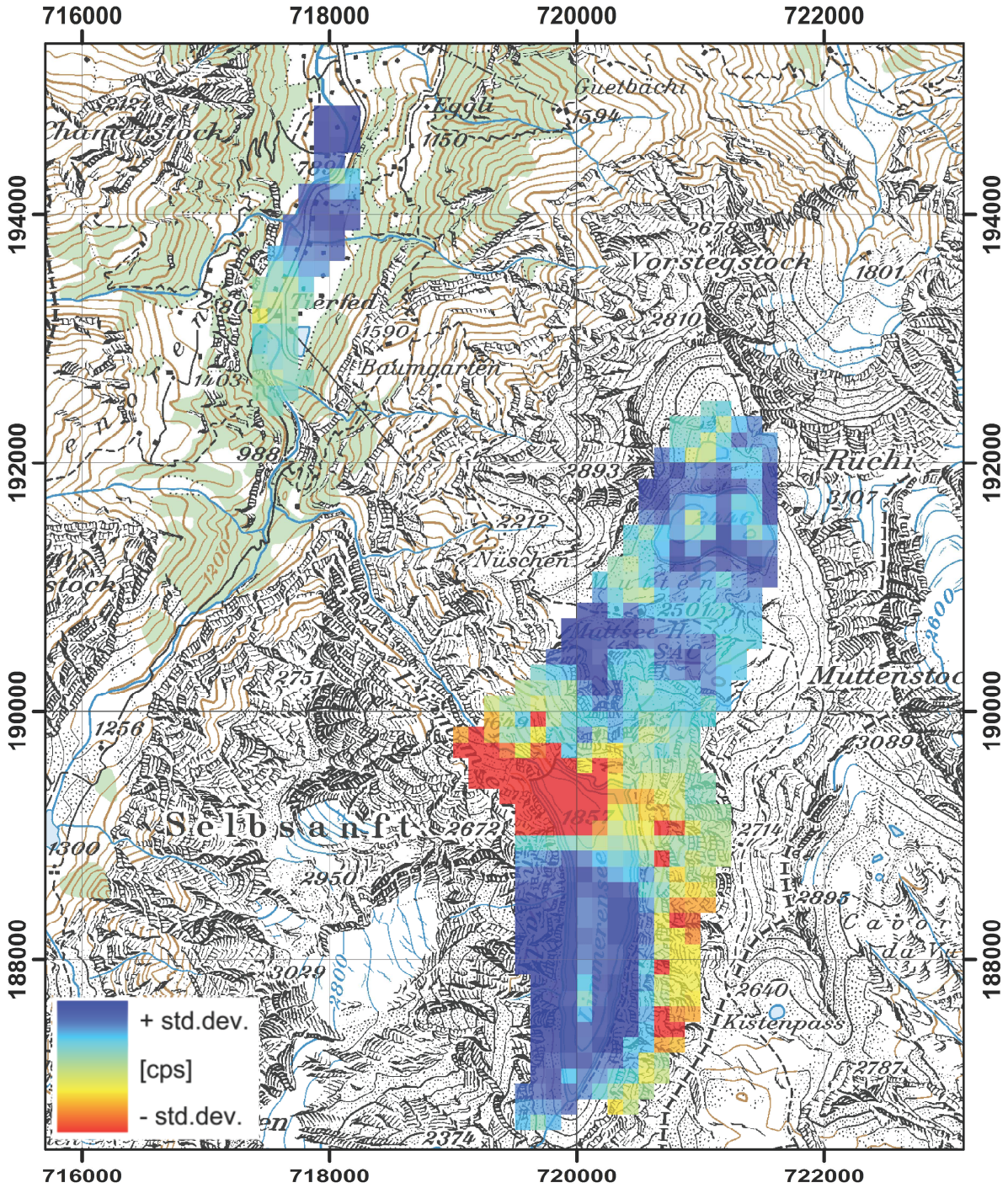

Figure 26: Variation of the count rate in the MMGC high energy window in the vicinity of Limmerensee.
PK100 © 2012 swisstopo (JD100042)

The count rate in the MMGC high energy window is the denominator used for the calculation of the MMGC ratio. The variation of the count rate in the MMGC high energy window (Figure 26) confirm that the high values of the MMGC ratio are artifacts produced by unusual low values of this count rate.

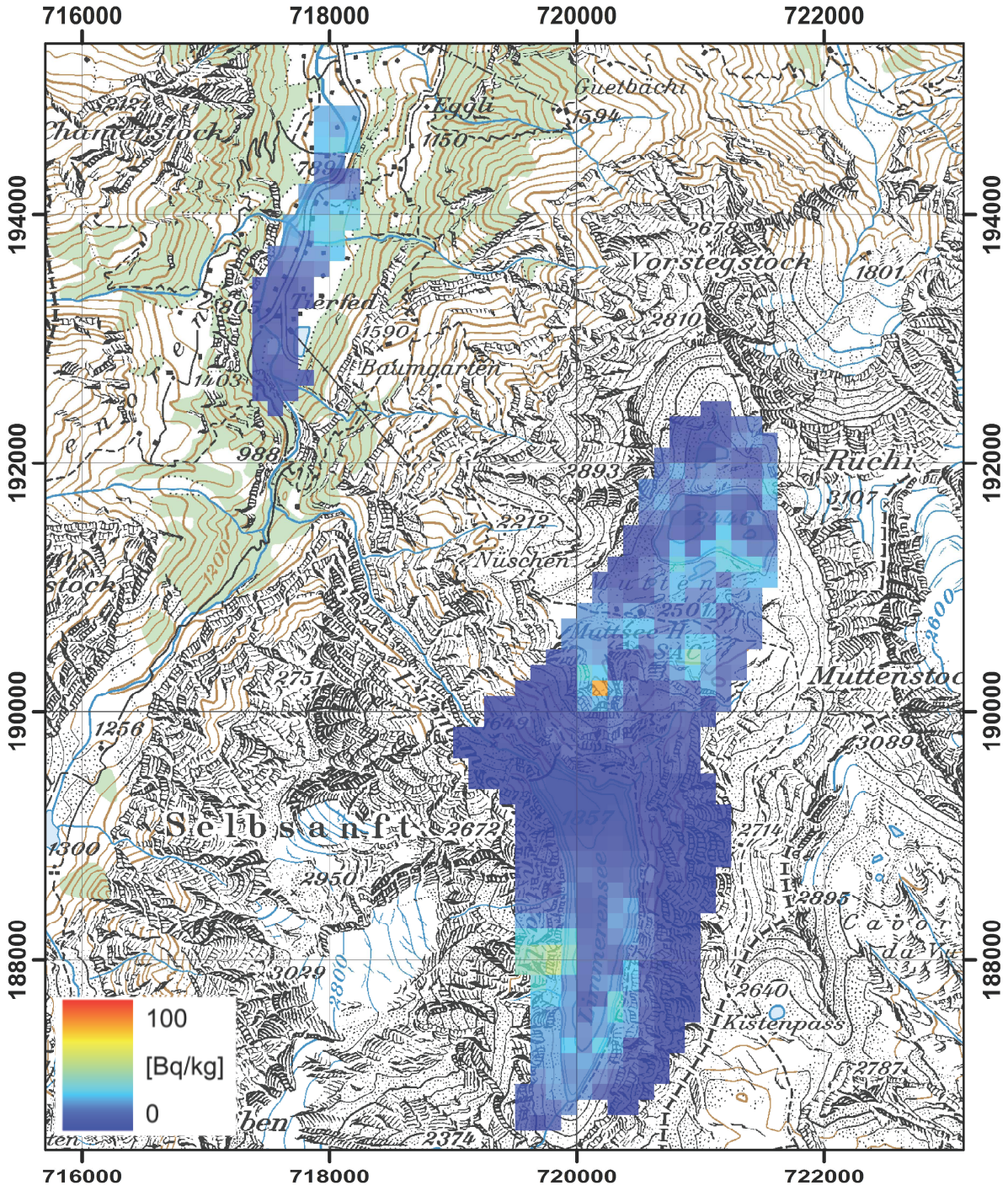

Figure 27: ^{232}Th activity concentration in the vicinity of Limmerensee. PK100 © 2012 swisstopo (JD100042)

The map of the ^{232}Th activity concentration (Figure 27) shows two areas with elevated values at coodinates (719780, 188020) and (720180, 190210).

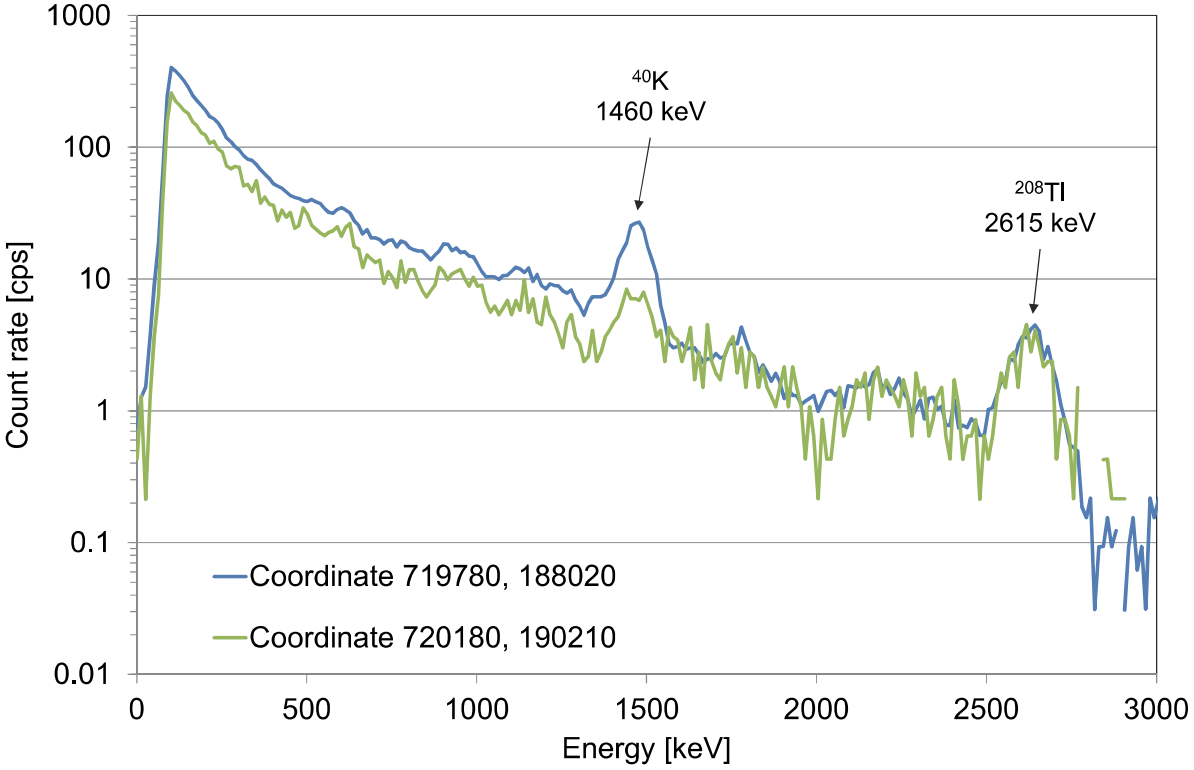

Figure 28: Photon spectra over the areas with elevated ^{232}Th activity concentrations.

The photon spectra averaged over the two areas with elevated ^{232}Th concentrations (Figure 28) indicate at the southern of these two points also elevated values of the natural radionuclide ^{40}K.

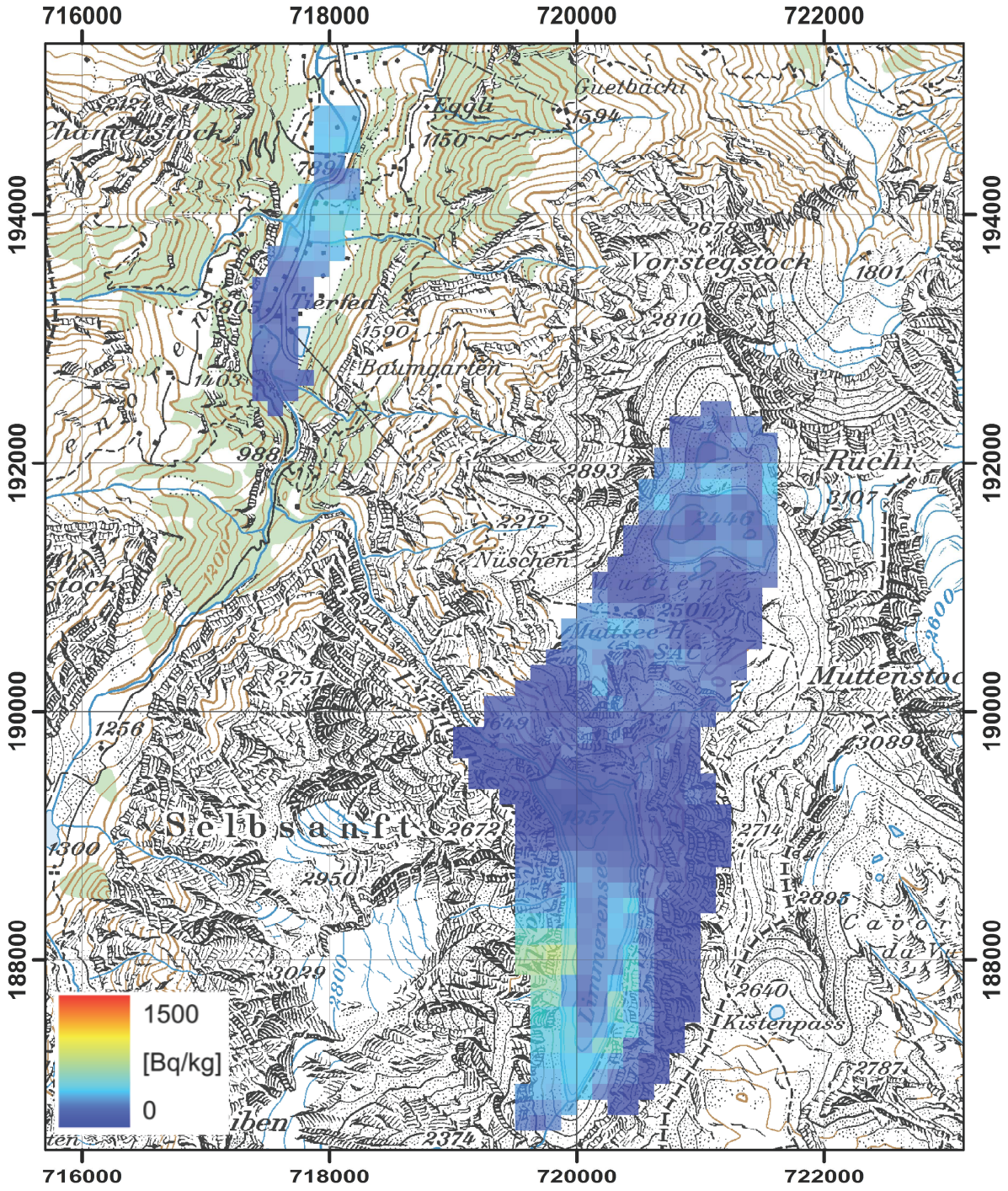

Figure 29: ^{40}K activity concentration in the vicinity of Limmerensee. PK100 © 2012 swisstopo (JD100042)

As suggested from the photon spectra (Figure 28), elevated ^{40}K concentrations are observed over the southern point with increased ^{232}Th activity concentrations (Figure 29).

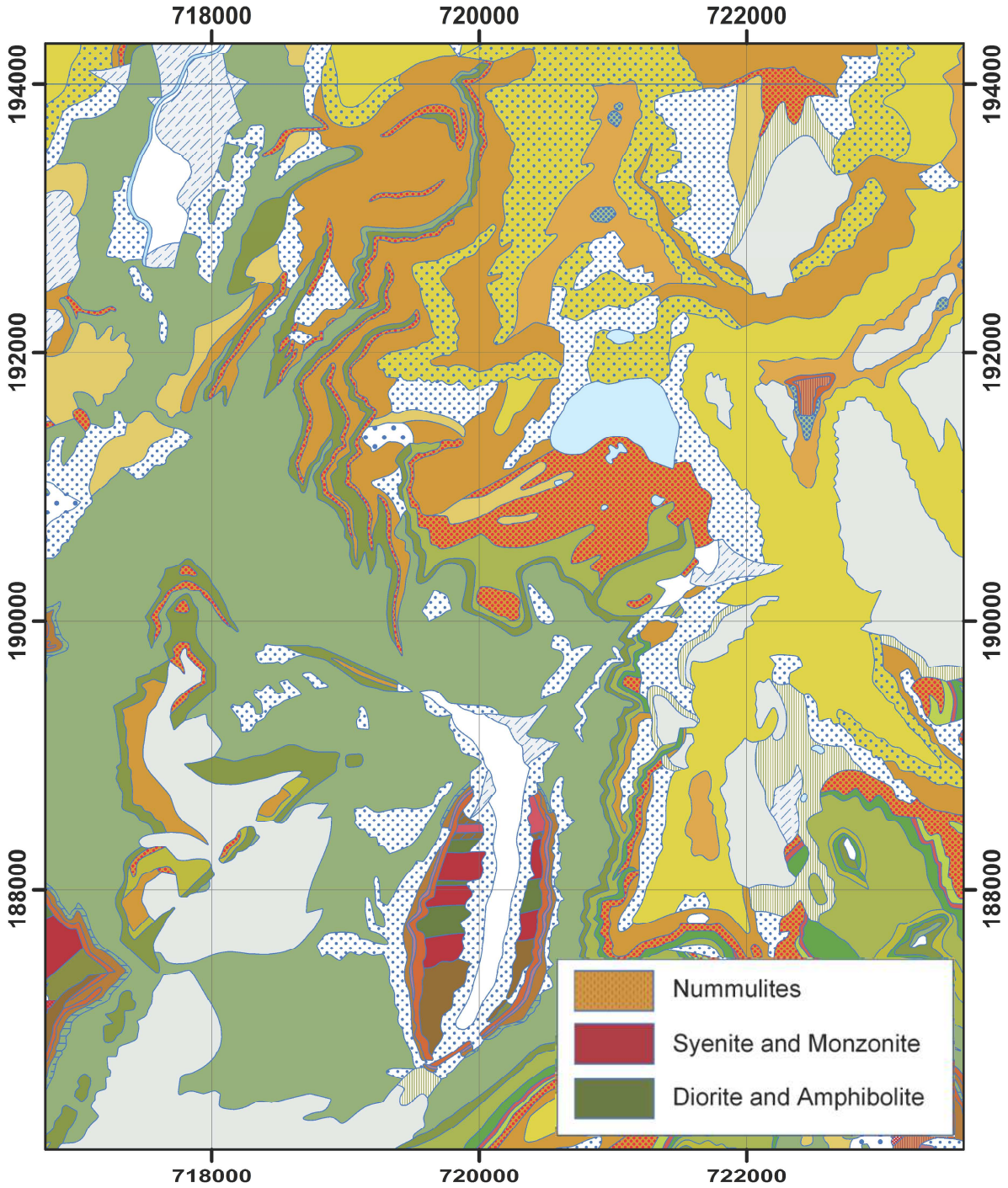

Figure 30: Geological map of the vicinity of Limmerensee.
GeoCover © 2012 swisstopo (JD100042)

The elevated values of the ^{40}K activity concentration (Figure 29) correspond in the southern part well with the distribution of layers from syenite, monzonite, diorite and amphibolite (Figure 30). The northern spot with elevated ^{232}Th activity concentration (Figure 27) at coordinate (720180, 190210) is located over a layer of nummulites, a rock formation with no reports of enriched thorium concentrations. As this point is located at a mountain peak, a topographical artifact can not be excluded.

2.6 Profile Weinfelden – Great St. Bernhard

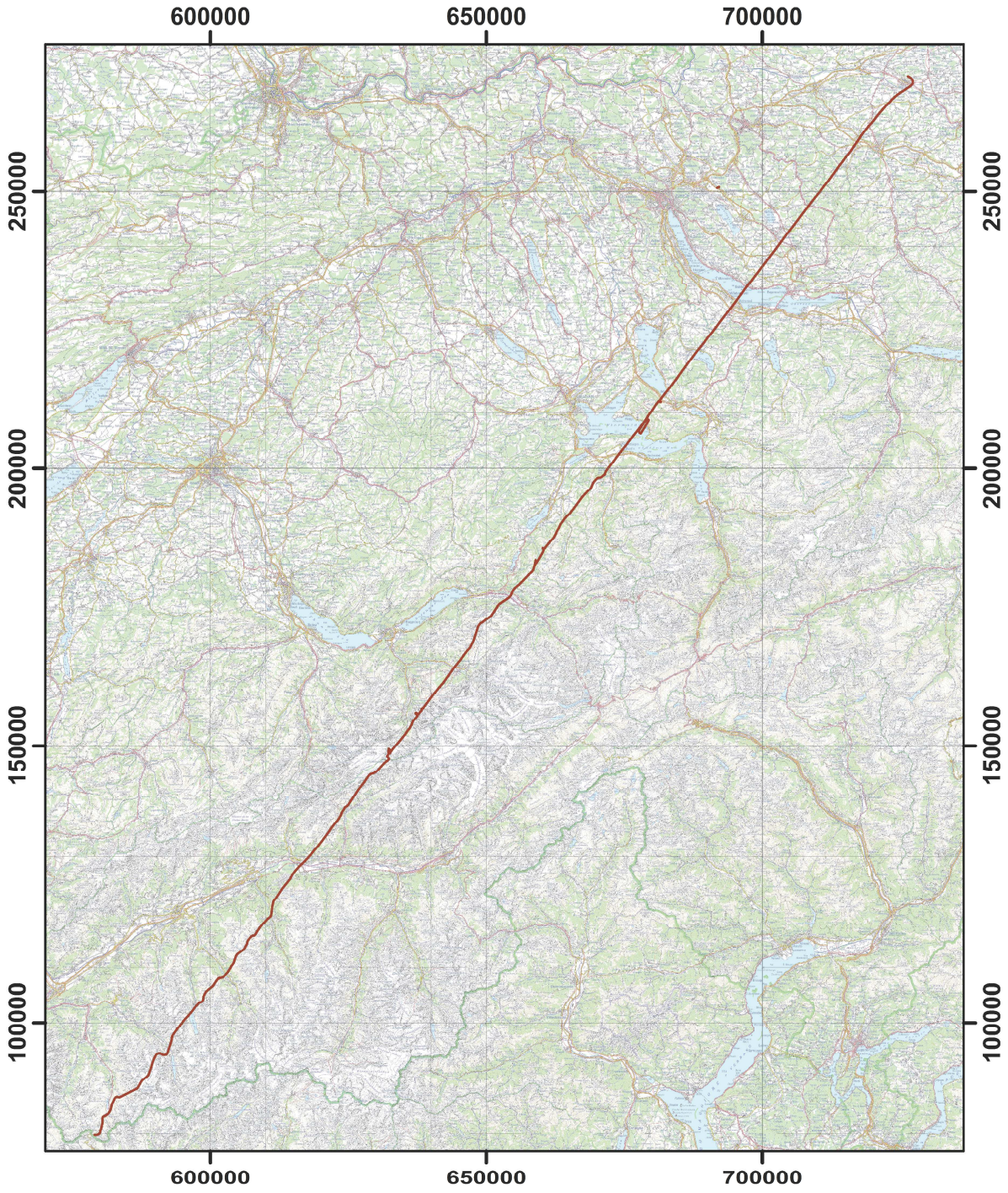

Figure 31: Flight line of the measured profile.
PK200 © 2012 swisstopo (JD100042)

A profile between Weinfelden in north-eastern Switzerland to the Great St. Bernhard in south-western Switzerland was measured aeroradiometrically to complement the existing data base of Swiss radiological data (Figure 31).

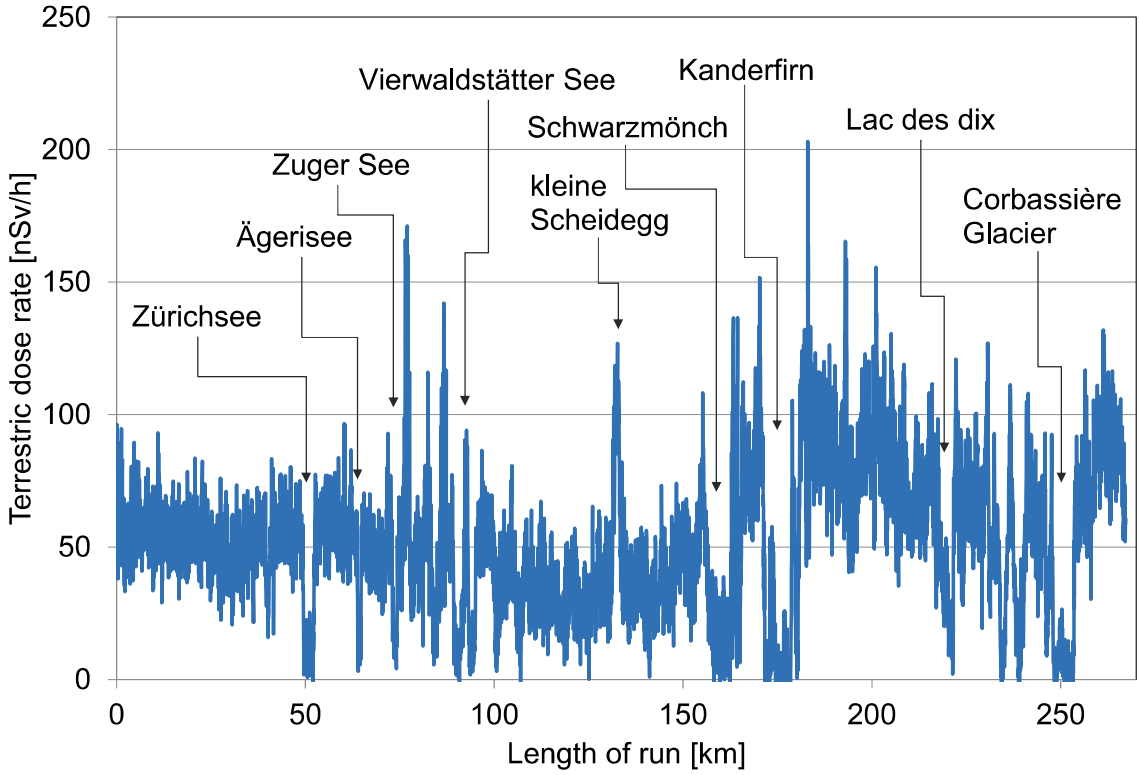

Figure 32: Terrestric dose rate along the profile from Weinfelden to Great St. Bernhard.

The terrestrial component of the dose rate along the flight line (Figure 32) of the profile from Weinfelden to Great St. Bernhard shows mainly the influence of the attenuation of photon radiation in the water layer of lakes and rivers. At some high alpine locations the attenuation in the ice of glaciers and snow fields is observed. The increase of the terrestric dose rate in southern Switzerland compared to the regions north of the Alps is correlated to the more frequent occurrence of metamorphic rock formations like granite and gneiss in southern Switzerland.

3 CONCLUSIONS

The measurement over the nuclear power plants Beznau (KKB) and Leibstadt (KKL), following a bi-annual routine showed no artificial radionuclides outside of the plant premises. As in previous years, the distinction between pressurized and boiling water reactor is clearly identified from the photon spectra. The intermediate storage facility ZWILAG could not be detected with airborne gamma-spectrometry.
Due to the intersection of the flight line with air discharged from the stack of the accelerators located at the western part of the Paul Scherrer Institut (PSI) a clear signal is observed over PSI. The detected radionuclides are a controlled and permitted release from the stack of PSI West.
Measurements over Zurich city and the freight yard near Spreitenbach showed homogeneous results at background level.
The aeroradiometric results near Lac d'Emosson and Limmerensee reflect the alpine

topography and local geological features.
A terrestrial dose rate profile from Weinfelden to the Great St. Bernhard is mainly characterized by the attenuation of photons from natural radionuclides in water bodies, glaciers and snow fields.

4 LITERATURE

Labhart, T.P. and Rybach, L.: Granite und Uranvererzungen in den Schweizer Alpen, Geol. Rundschau 63/1, 135-147, 1974.

Schwarz, G. F.: Methodische Entwicklungen zur Aerogammaspektrometrie. Beiträge zur Geologie der Schweiz, Geophysik Nr. 23, Schweizerische Geophysikalische Kommission, 1991.

Bucher, B.: Methodische Weiterentwicklungen in der Aeroradiometrie. Dissertation Nr. 13973, ETH Zürich, 2001.

5 PREVIOUS REPORTS

Schwarz, G. F., Klingelé, E. E., Rybach, L.: Aeroradiometrische Messungen in der Umgebung der schweizerischen Kernanlagen. Bericht für das Jahr 1989 zuhanden der Hauptabteilung für die Sicherheit der Kernanlagen (HSK). Interner Bericht, Institut für Geophysik, ETH Zürich, 1990.

Schwarz, G. F., Klingelé, E. E., Rybach, L.: Aeroradiometrische Messungen in der Umgebung der schweizerischen Kernanlagen. Bericht für das Jahr 1990 zuhanden der Hauptabteilung für die Sicherheit der Kernanlagen (HSK). Interner Bericht, Institut für Geophysik, ETH Zürich, 1991.

Schwarz, G. F., Klingelé, E. E., Rybach, L.: Aeroradiometrische Messungen in der Umgebung der schweizerischen Kernanlagen. Bericht für das Jahr 1991 zuhanden der Hauptabteilung für die Sicherheit der Kernanlagen (HSK). Interner Bericht, Institut für Geophysik, ETH Zürich, 1992.

Schwarz, G. F., Klingelé, E. E., Rybach, L.: Aeroradiometrische Messungen in der Umgebung der schweizerischen Kernanlagen. Bericht für das Jahr 1992 zuhanden der Hauptabteilung für die Sicherheit der Kernanlagen (HSK). Interner Bericht, Institut für Geophysik, ETH Zürich, 1993.

Schwarz, G. F., Klingelé, E. E., Rybach, L.: Aeroradiometrische Messungen in der Umgebung der schweizerischen Kernanlagen. Bericht für das Jahr 1993 zuhanden der Hauptabteilung für die Sicherheit der Kernanlagen (HSK). Interner Bericht, Institut für Geophysik, ETH Zürich, 1994.

Schwarz, G. F., Rybach, L.: Aeroradiometrische Messungen im Rahmen der Übung ARM94. Bericht für das Jahr 1994 zuhanden der Fachgruppe Aeroradiometrie (FAR). Interner Bericht, Institut für Geophysik, ETH Zürich, 1995.

Schwarz, G. F., Rybach, L.: Aeroradiometrische Messungen im Rahmen der Übung ARM95. Bericht für das Jahr 1995 zuhanden der Fachgruppe Aeroradiometrie (FAR). Interner Bericht, Institut für Geophysik, ETH Zürich, 1996.

Schwarz, G. F., Rybach, L., Bärlocher, C.: Aeroradiometrische Messungen im Rahmen der Übung ARM96. Bericht für das Jahr 1996 zuhanden der Fachgruppe Aeroradiometrie (FAR). Interner Bericht, Institut für Geophysik, ETH Zürich, 1997.

Bucher, B., Rybach, L., Schwarz, G., Bärlocher, C.: Aeroradiometrische Messungen im Rahmen der Übung ARM97. Bericht für das Jahr 1997 zuhanden der Fachgruppe Aeroradiometrie (FAR). Interner Bericht, Institut für Geophysik, ETH Zürich, 1998.

Bucher, B., Rybach, L., Schwarz, G., Bärlocher, C.: Aeroradiometrische Messungen im Rahmen der Übung ARM98. Bericht für das Jahr 1998 zuhanden der Fachgruppe Aeroradiometrie (FAR). Interner Bericht, Institut für Geophysik, ETH Zürich, 1999.

Bucher, B., Rybach, L., Schwarz, G., Bärlocher, C.: Aeroradiometrische Messungen im Rahmen der Übung ARM99. Bericht für das Jahr 1999 zuhanden der Fachgruppe Aeroradiometrie (FAR). Interner Bericht, Institut für Geophysik, ETH Zürich, 2000.

Bucher, B., Rybach, L., Schwarz, G., Bärlocher, C.: Aeroradiometrische Messungen im Rahmen der Übung ARM00. Bericht für das Jahr 2000 zuhanden der Fachgruppe Aeroradiometrie (FAR). Interner Bericht, Institut für Geophysik, ETH Zürich, 2001.

Bucher, B., Rybach, L., Schwarz, G., Bärlocher, C.: Aeroradiometrische Messungen im Rahmen der Übung ARM01. Bericht für das Jahr 2001 zuhanden der Fachgruppe Aeroradiometrie (FAR). Interner Bericht, Paul Scherrer Institut, Villigen, Schweiz, 2002.

Bucher, B., Rybach, L., Schwarz, G., Bärlocher, C.: Aeroradiometrische Messungen im Rahmen der Übung ARM02. Bericht für das Jahr 2002 zuhanden der Fachgruppe Aeroradiometrie (FAR). Interner Bericht, Paul Scherrer Institut, Villigen, Schweiz, 2003.

Bucher, B., Rybach, L., Schwarz, G.: Aeroradiometrische Messungen im Rahmen der Übung ARM03. PSI-Bericht 04-14, ISSN 1019-0643, Paul Scherrer Institut, Villigen, Schweiz, 2004.

Bucher, B., Butterweck, G., Rybach, L., Schwarz, G.: Aeroradiometrische Messungen im Rahmen der Übung ARM04. PSI-Bericht 05-10, ISSN 1019-0643, Paul Scherrer Institut, Villigen, Schweiz, 2005.

Bucher, B., Butterweck, G., Rybach, L., Schwarz, G.: Aeroradiometrische Messungen im Rahmen der Übung ARM05. PSI-Bericht 06-06, ISSN 1019-0643, Paul Scherrer Institut, Villigen, Schweiz, 2006.

Bucher, B., Butterweck, G., Rybach, L., Schwarz, G.: Aeroradiometrische Messungen im Rahmen der Übung ARM06. PSI-Bericht 07-02, ISSN 1019-0643, Paul Scherrer Institut, Villigen, Schweiz, 2007.

Bucher, B., Guillot, L., Strobl, C., Butterweck, G., Gutierrez, S., Thomas, M., Hohmann, C., Krol, I., Rybach, L., Schwarz, G.: International Intercomparison Exercise of Airborne Gammaspectrometric Systems of Germany, France and Switzerland in the Framework of the Swiss Exercise ARM07. PSI-Bericht Nr. 09-07, ISSN 1019-0643, Paul Scherrer Institut, Villigen, Schweiz, 2009.

Bucher, B., Butterweck, G., Rybach, L., Schwarz, G.: Aeroradiometrische Messungen im Rahmen der Übung ARM08. PSI-Bericht Nr. 09-02, ISSN 1019-0643, Paul Scherrer Institut, Villigen, Schweiz, 2009.

Bucher, B., Butterweck, G., Rybach, L., Schwarz, G., Strobl, C.: Aeroradiometrische Messungen im Rahmen der Übung ARM09. PSI-Bericht Nr. 10-01, ISSN 1019-0643, Paul Scherrer Institut, Villigen, Schweiz, 2010.

Bucher, B., Butterweck, G., Rybach, L., Schwarz, G., Mayer, S.: Aeroradiometrische Messungen im Rahmen der Übung ARM10. PSI-Bericht Nr. 11-02, ISSN 1019-0643, Paul Scherrer Institut, Villigen, Schweiz, 2011.

Bucher, B., Butterweck, G., Rybach, L., Schwarz, G., Mayer, S.: Aeroradiometric Measurements in the Framework of the Swiss Exercise ARM11. PSI-Report No. 12-04, ISSN 1019-0643, Paul Scherrer Institut, Villigen, Switzerland, 2012.

The reports since 1994 can be found and downloaded from the FAR website http://www.far.ensi.ch.

6 EVALUATION PARAMETER FILES

Starting with this year, the parameter files used for the evaluation of raw data are listed in this report to improve the traceability of the presented results. Additionally, the parameter files used in previous years are listed in this report.

6.1 DefinitionFile_Processing.txt

This file defines the parameters used for the gridding of evaluated parameters.

```
---------- Start of file ----------
Definition file Swiss MGS32
"Windows"
10
Total    401.    2997.      0.   0
K-40    1369.    1558.   1460.   1
U-238   1664.    1853.   1765.   1
Th-232  2407.    2797.   2615.   1
Cs-137   600.     720.    660.   2
Co-60   1100.    1400.      0.   2
MMGC1    400.    1400.      0.   0
MMGC2   1400.    2997.      0.   0
LOW       40.     720.      0.   0
MID      720.    2997.      0.   0
"Ratios"
3
MMGCVerhältnis   MMGC1  MMGC2  Ratio_MMGC
LOWHigh          LOW    MMGC2  RatioLowHigh
LowMid           LOW    MID    RatioLowMid
```

```
"Conversion factors Activity to Dose Rate"
8
Total       0        NoCalibration   "     "   0
AD_K-40        0.044    DHSR           "nSv/h"   1
AD_U-238       0.55     DHSR           "nSv/h"   1
AD_Th-232      0.77     DHSR           "nSv/h"   1
AD_Cs-137      0.2      DHSR           "nSv/h"   2
Co-60       0        NoCalibration   "     "   0
MMGC1       0        NoCalibration   "     "   0
MMGC2       0        NoCalibration   "     "   0
"Typ des Darstellungsgrenzwertes"
1
Nachweistyp  0
"counts of spectra to stack"
1
Counts 1
"Auszugebende Werte"
30
"DHSR TOT            ","DHSR_TOT","nSv/h       ",0.00,250.00
"AP_Co-60            ","AP_Co-60","MBq         ",0.00,150.00
"AP_Cs-137           ","AP_Cs-137","MBq        ",0.00,40.00
"Terr. DL            ","DHSR_TOT","nSv/h      ",0.00,250.00
"CR_Caesium          ","CR_Cs-137","cps        ",20.00,120.00
"CR_Cobalt           ","CR_Co-60","cps         ",0.00,100.00
"Low-HighRatio       ","RatioLowHigh","%       ",0.00,1000.00
"Low-MidRatio        ","RatioLowMid","%        ",0.00,1000.00
"Total_CR_corr       ","NR_Total","cps         ",200.00,1200.00
"K-40               ","AD_K-40","Bq/kg      ",0.00,1000.00
"U-238              ","AD_U-238","Bq/kg      ",0.00,120.00
"Th-232             ","AD_Th-232","Bq/kg     ",0.00,120.00
"Cs-137             ","AD_Cs-137","Bq/kg     ",0.00,240.00
"Cobalt_CR          ","NR_Co-60","cps        ",0.00,120.00
"Nat.Terr.DL        ","DHSR_NAT","nSv/h      ",0.00,250.00
"Künst.DL           ","DHSR_ANT","nSv/h      ",0.00,250.00
"MMGC_Ratio         ","MMGC_Ratio","%        ",400,600.00
"Cosmic DL          ","DHSR_COS","nSv/h      ",20.00,60.00
"Cosmic             ","CR_COS","cps          ",000.00,400.00
"Radar              ","PH","m          ",0.00,300.00
"ODL                ","DHSR","nSv/h      ",0.00,250
"AD_UT_K-40         ","AD_UT_K-40","Bq/kg     ",0.00,200
"CR_MMGC2           ","CR_MMGC2","cps         ",0.00,1000.00
"AD_UT_Th-232       ","AD_UT_Th-232","Bq/kg      ",0.00,40
"AD_UT_Cs-137       ","AD_UT_Cs-137","Bq/kg      ",0.00,20
"Err_Co-60          ","NR_UT_Co-60","cps         ",0.00,40
"Nachweis_Cs-137     ","CR_LD_Cs-137,"cps         ",0.00,100.00
"Nachweis_Co-60      ","CR_LD_Co-60","cps         ",0.00,100.00
"Cs-137 beta=0       ","AA_Cs-137","Bq/m2      ",0.00,20000.00
"AA_UT_Cs-137        ","AA_UT_Cs-137","Bq/m2      ",0.00,20
```

---------- End of file ----------

6.2 DefinitionFile_DetC.txt

This file defines the parameters used for the derivation of dose rates and activity concentrations from the raw spectra. The current file is customized for the 16-litre-detector purchased from Exploranium in the year 2007. This detector was used in all measurements since the year 2007.

```
---------- Start of file ----------
Definition file System
"Koordinaten"
WGS84
"Non-linearity"
4
a0  0.6966
a1  0.08423
a2  -0.0000032807
a3  0.00000000042937
"Recorder old RDT-Files"
8
Radar  0.00   -61.00
Baro   0.74   457.14
Cosm   0.00   1.00
Dead   5.00   0.00
Time   0.00   1.00
Temp   0.00   1.00
Pitch  0.00   76.20
Roll   0.00   90.91
"Background/Cosmic"
10
Total      98.1000       1.041      0.032
K-40        12.100       0.050      0.004
U-238        2.700       0.043      0.002
Th-232       3.400       0.044      0.001
Cs-137      15.500       0.102      0.005
Co-60       13.900       0.100      0.004
MMGC1       79.540       0.771      0.019
MMGC2       18.500       0.270      0.007
LOW          0.          0.         0.
MID          0.          0.         0.
"Stripping Coefficients"
10
1.000  0.000  0.000  0.000  0.000  0.000  0.000  0.000  0.000  0.000
0.000  1.000  0.710  0.350  0.000  0.070  0.000  0.000  0.000  0.000
0.000 -0.020  1.000  0.210  0.000 -0.010  0.000  0.000  0.000  0.000
0.000 -0.010  0.040  1.000  0.000  0.000  0.000  0.000  0.000  0.000
0.000  0.060  3.760  2.340  1.000  0.170  0.000  0.000  0.000  0.000
0.000  0.280  2.360  0.550  0.000  1.000  0.000  0.000  0.000  0.000
0.000  0.000  0.000  0.000  0.000  0.000  1.000  0.000  0.000  0.000
0.000  0.000  0.000  0.000  0.000  0.000  0.000  1.000  0.000  0.000
0.000  0.000  0.000  0.000  0.000  0.000  0.000  0.000  1.000  0.000
```

0.000 0.000 0.000 0.000 0.000 0.000 0.000 0.000 0.000 1.000
"Converted Stripping Coefficients Matrix"
10
1.000 0.000 0.000 0.000 0.000 0.000 0.000 0.000 0.000 0.000
0.000 1.030 -0.730 -0.200 0.000 -0.070 0.000 0.000 0.000 0.000
0.000 0.020 0.980 -0.340 0.000 0.010 0.000 0.000 0.000 0.000
0.000 0.010 -0.050 1.010 0.000 0.000 0.000 0.000 0.000 0.000
0.000 -0.280 -3.230 -1.180 1.000 -0.170 0.000 0.000 0.000 0.000
0.000 -0.700 -2.120 0.260 0.000 1.030 0.000 0.000 0.000 0.000
0.000 0.000 0.000 0.000 0.000 0.000 1.000 0.000 0.000 0.000
0.000 0.000 0.000 0.000 0.000 0.000 0.000 1.000 0.000 0.000
0.000 0.000 0.000 0.000 0.000 0.000 0.000 0.000 1.000 0.000
0.000 0.000 0.000 0.000 0.000 0.000 0.000 0.000 0.000 1.000
"Sigma of Converted Stripping Coefficients Matrix"
10
0.000 0.000 0.000 0.000 0.000 0.000 0.000 0.000 0.000 0.000
0.000 0.000 -0.040 -0.017 0.000 -0.016 0.000 0.000 0.000 0.000
0.000 0.000 0.000 -0.028 0.000 0.000 0.000 0.000 0.000 0.000
0.000 0.000 -0.009 0.000 0.000 0.000 0.000 0.000 0.000 0.000
0.000 -0.080 -0.103 -0.037 0.000 -0.008 0.000 0.000 0.000 0.000
0.000 -0.140 -0.068 0.013 0.000 0.000 0.000 0.000 0.000 0.000
0.000 0.000 0.000 0.000 0.000 0.000 0.000 0.000 0.000 0.000
0.000 0.000 0.000 0.000 0.000 0.000 0.000 0.000 0.000 0.000
0.000 0.000 0.000 0.000 0.000 0.000 0.000 0.000 0.000 0.000
0.000 0.000 0.000 0.000 0.000 0.000 0.000 0.000 0.000 0.000
"Attenuation Coefficients"
10
Total 0.00600 1.00000 0.0003
K-40 0.00800 1.00000 0.0008
U-238 0.00550 1.00000 0.0114
Th-232 0.00600 1.00000 0.0044
Cs-137 0.01000 1.00000 0.0100
Co-60 0.00800 1.00000 0.0080
MMGC1 0.00600 1.00000 0.0060
MMGC2 0.00650 1.00000 0.0065
LOW 0.02000 1.00000 0.01
MID 0.01500 1.00000 0.005
"3D Attenuation Coefficients"
10
Total 0.00350 2.00000
K-40 0.00420 2.00000
U-238 0.00320 2.00000
Th-232 0.00350 2.00000
Cs-137 0.00800 2.00000
Co-60 0.00800 1.00000
MMGC1 0.00600 1.00000
MMGC2 0.00650 1.00000
LOW 0.02000 1.00000
MID 0.01500 1.00000

```
"Conversion factors Counts to Activity"
9
Total       0       NoCalibration   "     "
K-40        7.95     AD_K-40         "Bq/kg"
U-238       3.87     AD_U-238        "Bq/kg"
Th-232      1.62     AD_Th-232       "Bq/kg"
Cs-137      1.88     AD_Cs-137       "Bq/kg"
Cs-137      32.96    AA_Cs-137       "Bq/m2"
Co-60       0       NoCalibration   "     "
MMGC1       0       NoCalibration   "     "
MMGC2       0       NoCalibration   "     "
"Radon"
1
0          0
"Hoehenkorrektur"
3
1
1
PfadDHM25   K:\Aeroradiometrie\GammaMap\DHM25\
"SDI Constants"
7
Aten         0.0053
Convert      0.00096
CosmicKorr   95.5
Back         12640.0
Gain         12.0
referenz_alt 100.0
Threshold    240.0
----------------- End of file --------------------
```

6.3 DefinitionFile_DetA.txt

This file defines the parameters used for the derivation of dose rates and activity concentrations from the raw spectra. The file below is customized for the 16-litre-detector from Exploranium purchased in the year 1992. This detector was used in most of the measurements in the years 1992 to 2006.

```
----------------- Start of file --------------------
Definition file System
"Koordinaten"
WGS84
"Non-linearity"
4
a0  0.6966
a1  0.08423
a2  -0.0000032807
a3  0.00000000042937
"Recorder old RDT-Files"
```

8
Radar 0.00 -61.00
Baro 0.74 457.14
Cosm 0.00 1.00
Dead 5.00 0.00
Time 0.00 1.00
Temp 0.00 1.00
Pitch 0.00 76.20
Roll 0.00 90.91
"Background/Cosmic"
10
Total 98.1000 1.041 0.032
K-40 12.100 0.050 0.004
U-238 2.700 0.043 0.002
Th-232 3.400 0.044 0.001
Cs-137 15.500 0.102 0.005
Co-60 13.900 0.100 0.004
MMGC1 79.540 0.771 0.019
MMGC2 18.500 0.270 0.007
LOW 0. 0. 0.
MID 0. 0. 0.
"Stripping Coefficients"
10
1.000 0.000 0.000 0.000 0.000 0.000 0.000 0.000 0.000 0.000
0.000 1.000 0.690 0.280 0.000 0.150 0.000 0.000 0.000 0.000
0.000 0.000 1.000 0.200 0.000 0.000 0.000 0.000 0.000 0.000
0.000 0.000 0.050 1.000 0.000 0.000 0.000 0.000 0.000 0.000
0.000 0.130 3.870 1.820 1.000 0.120 0.000 0.000 0.000 0.000
0.000 0.300 1.960 0.390 0.000 1.000 0.000 0.000 0.000 0.000
0.000 0.000 0.000 0.000 0.000 0.000 1.000 0.000 0.000 0.000
0.000 0.000 0.000 0.000 0.000 0.000 0.000 1.000 0.000 0.000
0.000 0.000 0.000 0.000 0.000 0.000 0.000 0.000 1.000 0.000
0.000 0.000 0.000 0.000 0.000 0.000 0.000 0.000 0.000 1.000
"Converted Stripping Coefficients Matrix"
10
1.000 0.000 0.000 0.000 0.000 0.000 0.000 0.000 0.000 0.000
0.000 1.084 -0.505 -0.169 0.000 -0.163 0.000 0.000 0.000 0.000
0.000 0.000 1.014 -0.275 0.000 0.000 0.000 0.000 0.000 0.000
0.000 0.000 -0.051 1.014 0.000 0.000 0.000 0.000 0.000 0.000
0.000 -0.237 -3.600 -0.841 1.000 -0.084 0.000 0.000 0.000 0.000
0.000 -0.560 -1.894 0.125 0.000 1.084 0.000 0.000 0.000 0.000
0.000 0.000 0.000 0.000 0.000 0.000 1.000 0.000 0.000 0.000
0.000 0.000 0.000 0.000 0.000 0.000 0.000 1.000 0.000 0.000
0.000 0.000 0.000 0.000 0.000 0.000 0.000 0.000 1.000 0.000
0.000 0.000 0.000 0.000 0.000 0.000 0.000 0.000 0.000 1.000
"Sigma of Converted Stripping Coefficients Matrix"
10
0.000 0.000 0.000 0.000 0.000 0.000 0.000 0.000 0.000 0.000
0.000 0.000 -0.040 -0.017 0.000 -0.016 0.000 0.000 0.000 0.000

```
0.000  0.000  0.000 -0.028  0.000  0.000  0.000  0.000  0.000  0.000
0.000  0.000 -0.009  0.000  0.000  0.000  0.000  0.000  0.000  0.000
0.000 -0.080 -0.103 -0.037  0.000 -0.008  0.000  0.000  0.000  0.000
0.000 -0.140 -0.068  0.013  0.000  0.000  0.000  0.000  0.000  0.000
0.000  0.000  0.000  0.000  0.000  0.000  0.000  0.000  0.000  0.000
0.000  0.000  0.000  0.000  0.000  0.000  0.000  0.000  0.000  0.000
0.000  0.000  0.000  0.000  0.000  0.000  0.000  0.000  0.000  0.000
0.000  0.000  0.000  0.000  0.000  0.000  0.000  0.000  0.000  0.000
"Attenuation Coefficients"
10
Total       0.00600    1.00000   0.0003
K-40        0.00800    1.00000   0.0008
U-238       0.00550    1.00000   0.0114
Th-232      0.00600    1.00000   0.0044
Cs-137      0.01000    1.00000   0.0100
Co-60       0.00800    1.00000   0.0080
MMGC1       0.00600    1.00000   0.0060
MMGC2       0.00650    1.00000   0.0065
LOW         0.02000    1.00000   0.01
MID      0.01500    1.00000   0.005
"3D Attenuation Coefficients"
10
Total       0.00350    2.00000
K-40        0.00420    2.00000
U-238       0.00320    2.00000
Th-232      0.00350    2.00000
Cs-137      0.00800    2.00000
Co-60       0.00800    1.00000
MMGC1       0.00600    1.00000
MMGC2       0.00650    1.00000
LOW         0.02000    1.00000
MID         0.01500    1.00000
"Conversion factors Counts to Activity"
9
Total       0       NoCalibration   "     "
K-40        8.29     AD_K-40         "Bq/kg"
U-238       4.0      AD_U-238        "Bq/kg"
Th-232      1.67     AD_Th-232       "Bq/kg"
Cs-137      2.0      AD_Cs-137       "Bq/kg"
Cs-137      35.0     AA_Cs-137       "Bq/m2"
Co-60       0       NoCalibration   "     "
MMGC1       0        NoCalibration   "     "
MMGC2       0        NoCalibration   "     "
"Radon"
1
0          0
"Hoehenkorrektur"
3
1
```

```
1
PfadDHM25   K:\Aeroradiometrie\GammaMap\DHM25\
"SDI Constants"
7
Aten         0.0056
Convert      0.00096
CosmicKorr   95.5
Back         12640.0
Gain         12.0
referenz_alt 100.0
Threshold    240.0
------------------ End of file ---------------------
```

6.4 DefinitionFile_Detektor_klein.txt

This file defines the parameters used for the derivation of dose rates and activity concentrations from the raw spectra. The file below is customized for a 4-litre-detector from Exploranium. This detector was used for few measurements in the years 1996 and 2005.

```
------------------ Start of file ---------------------
Definition file Swiss MGS32
"Koordinaten"
WGS84
"Non-linearity"
4
a0  0.6966
a1  0.08423
a2  -0.0000032807
a3  0.00000000042937
"Recorder"
8
Radar  0.00   -61.00
Baro   0.74   457.14
Cosm   0.00   1.00
Dead   5.00   0.00
Time   0.00   1.00
Temp   0.00   1.00
Pitch  0.00   76.20
Roll   0.00   90.91
"Windows"
8
Total    401.    2997.    0.
Kalium   1369.   1558.   1460.
Uranium  1664.   1853.   1765.
Thorium  2407.   2797.   2615.
Caesium  600.    720.    660.
```

```
Kobalt   1100.    1400.      0.
MMGC1     400.    1400.      0.
MMGC2    1400.    2997.      0.
"Background/Cosmic"
8
Window1    24.5250       1.041      0.032
Window2      3.025       0.050      0.004
Window3      0.675       0.043      0.002
Window4      0.850       0.044      0.001
Window5      3.875       0.102      0.005
Window6      3.475       0.100      0.004
Window7     19.890       0.771      0.019
Window8      4.625       0.270      0.007
"Stripping Coefficients"
8
1.000  0.000  0.000  0.000  0.000  0.000  0.000  0.000
0.000  1.000  0.690  0.280  0.000  0.150  0.000  0.000
0.000  0.000  1.000  0.200  0.000  0.000  0.000  0.000
0.000  0.000  0.050  1.000  0.000  0.000  0.000  0.000
0.000  0.130  3.870  1.820  1.000  0.120  0.000  0.000
0.000  0.300  1.960  0.390  0.000  1.000  0.000  0.000
0.000  0.000  0.000  0.000  0.000  0.000  1.000  0.000
0.000  0.000  0.000  0.000  0.000  0.000  0.000  1.000
"Converted Stripping Coefficients Matrix"
8
1.000  0.000  0.000  0.000  0.000  0.000  0.000  0.000
0.000  1.084 -0.505 -0.169  0.000 -0.163  0.000  0.000
0.000  0.000  1.014 -0.275  0.000  0.000  0.000  0.000
0.000  0.000 -0.051  1.014  0.000  0.000  0.000  0.000
0.000 -0.237 -3.600 -0.841  1.000 -0.084  0.000  0.000
0.000 -0.560 -1.894  0.125  0.000  1.084  0.000  0.000
0.000  0.000  0.000  0.000  0.000  0.000  1.000  0.000
0.000  0.000  0.000  0.000  0.000  0.000  0.000  1.000
"Sigma of Converted Stripping Coefficients Matrix"
8
0.000  0.000  0.000  0.000  0.000  0.000  0.000  0.000
0.000  0.000 -0.040 -0.017  0.000 -0.016  0.000  0.000
0.000  0.000  0.000 -0.028  0.000  0.000  0.000  0.000
0.000  0.000 -0.009  0.000  0.000  0.000  0.000  0.000
0.000 -0.080 -0.103 -0.037  0.000 -0.008  0.000  0.000
0.000 -0.140 -0.068  0.013  0.000  0.000  0.000  0.000
0.000  0.000  0.000  0.000  0.000  0.000  0.000  0.000
0.000  0.000  0.000  0.000  0.000  0.000  0.000  0.000
"Attenuation Coefficients"
8
Window1     0.00600    1.00000   0.0003
Window2     0.00800    1.00000   0.0008
Window3     0.00550    1.00000   0.0114
Window4     0.00600    1.00000   0.0044
```

```
Window5     0.01000    1.00000   0.0100
Window6     0.00800    1.00000   0.0080
Window7     0.00600    1.00000   0.0060
Window8     0.00650    1.00000   0.0065
"3D Attenuation Coefficients"
8
Window1     0.00350    2.00000
Window2     0.00420    2.00000
Window3     0.00320    2.00000
Window4     0.00350    2.00000
Window5     0.00800    2.00000
Window6     0.00800    1.00000
Window7     0.00600    1.00000
Window8     0.00650    1.00000
"Conversion factors Counts to Activity"
4
Kalium      33.16
Uran        16.0
Thorium     6.68
Caesium     8.0
"Conversion factors Activity to Dose Rate"
4
Kalium      0.04
Uran        0.5
Thorium     0.71
Caesium     0.17
"Radon"
1
0           0
"Hoehenkorrektur"
3
0
1
PfadDHM25   C:\Users\Benno\Aeroradiometrie\Daten\DHM25\
"SDI Constants"
7
Aten        0.0056
Convert     0.00384
CosmicKorr  95.5
Back        3160.0
Gain        12.0
referenz_alt 100.0
Threshold   240.0
"Typ des Darstellungsgrenzwertes"
1
Nachweistyp  0
------------------ End of file ----------------------
```

Paul Scherrer Institut, 5232 Villigen PSI, Switzerland
Tel. +41 56 310 21 11, Fax +41 56 310 21 99
www.psi.ch